T_b or not T_b: Banding in Turbidite Sandstones

Christopher J Stevenson[1*], Jeff Peakall[2], David M Hodgson[2], Daniel Bell[3], Aurelia Privat[2]

[1]School of Earth and Ocean Sciences, University of Liverpool,

[2]School of Earth and Environment, University of Leeds, LS2 9JT

[3]School of Earth and Environmental Sciences, University of Manchester, Manchester M13 9PL, U.K.

*Corresponding author: Christopher.Stevenson@liverpool.ac.uk

ABSTRACT

Recognition and interpretation of sedimentary structures is fundamental to understanding sedimentary processes. Banded sandstones are an enigmatic sedimentary facies comprising alternating mud-rich (as matrix and/or mud clasts) and cleaner sand layers. The juxtaposition of hydrodynamically different grain sizes contradicts established models of cleaner sand bedform development. Here, outcrop, subsurface core, and petrographic data from three deep-water systems, with well-constrained paleogeographic contexts, are used to describe the range of sedimentary textures, bedform morphologies and facies associations, and to quantify the mud content of banding. Banding can occur in any part of a bed (base, middle or top), but typically overlies a structureless basal sandstone or mud clast conglomerate lag, and is overlain by clean parallel-laminated sandstone and/or ripple cross-lamination. Banding morphology ranges from sub-parallel to bedforms that comprise low-angle laminae with discontinuous lenses of mudstone, or asymmetric bedforms comprising steeply dipping foresets that transition downstream into low-amplitude bedwaves, or steeply dipping ripple-like bedforms with heterolithic foresets. This style of banding is interpreted as a range of bedforms that form progressively within the upper stage plane

bed flow regime via tractional reworking beneath mud-laden transitional plug flows. The balance of cohesive and turbulent forces, and the rate of flow deceleration (aggradation rate), govern the style of deposit. Banded sandstones and linked-debrites are rarely found juxtaposed together in the same bed as they are distributed preferentially in proximal and distal settings, respectively. Understanding the origins of banding in turbidite sandstones, the conditions under which it forms, and its distribution across deep-water systems and relationship to linked-debrites, is important for it to be used effectively as a tool to interpret the geological record.

INTRODUCTION

Banded sandstones have been described as alternating light (cleaner) and dark (mud-rich; as matrix and/or mud clasts) parallel, sub-parallel or wavy layers within an otherwise clean turbidite sandstone (e.g., Lowe and Guy, 2000; Lowe et al., 2003; Haughton et al., 2009; Hofstra et al., 2015, 2018). Our process understanding of banding is largely derived from analysis of deep-water deposits in the Lower Cretaceous Britannia Formation and Paleogene Forties Fan in the North Sea (Blackbourn and Thomson, 2000; Lowe and Guy, 2000; Lowe et al., 2003; Barker et al., 2008; Davis et al., 2009; Haughton et al., 2009). Typically, banded sandstone divisions within the Britannia Formation are thick (up to several meters) and occur overlying clean structureless basal sandstones (Fig. 1; Guy, 1992; Blackbourn and Thomson, 2000; Lowe and Guy, 2000; Lowe et al., 2003; Barker et al., 2008). Individual bands range in thickness from a few millimeters (microbanding), through 1-10 cm (mesobanding) and 10-50 cm (macrobanding), to >50 cm (megabanding) (Fig. 1). Banding documented within the Paleogene Forties Fan is restricted to relatively thin divisions (up to 15 cm) of microbanding that are sandwiched between a clean basal sandstone and an overlying linked debrite; collectively forming hybrid event beds (Fig. 1; *sensu* Haughton et al., 2009). This style of

48 banding has also been reported from the Ross Formation, Ireland (Pierce et al., 2018) and the
49 Springar Formation., North Sea (Southern et al., 2017).

50

51 However, these data have important limitations. First, descriptions of banding are based on 10 cm
52 wide core, which inhibits recognition of larger wavelength bedforms. Therefore, it is entirely possible
53 that banding may comprise a more diverse range of bedforms, which would be identifiable in more
54 laterally extensive datasets. Second, there has been a limited amount of thin-section analysis of
55 banded sandstones published, which is restricted to averaged textural properties of both the light
56 and dark layers in the banded divisions (Lowe and Guy, 2000; Sylvester and Lowe, 2004). The
57 composition of individual bands is poorly quantified, which limits our ability to recognize banding in
58 the field, interpret its formational processes, and distinguish it from conventional sedimentary
59 structures, such as planar lamination (Bouma T_b division).

60

61 Banded sandstones have been documented within a variety of deep-water depositional
62 environments, occurring in either relatively proximal settings with clean sandstones (Kane and
63 Pontén, 2012; Hofstra et al., 2015, 2018; Spychala et al., 2017) or rarely in association with hybrid
64 beds in distal settings (Southern et al., 2017; Fonnesu et al., 2018), and specifically fan fringe settings
65 (Davis et al., 2009; Haughton et al., 2009; Pierce et al., 2018). Field observations of micro- to
66 mesobanding indicate that bands can be continuous, show thickness variations, or be discontinuous
67 over meters (Hofstra et al., 2015, 2018; Spychala et al., 2017; Fonnesu et al., 2018). Furthermore,
68 their morphology can be parallel, sub-parallel or wavy (Hofstra et al., 2015, 2018). Despite these
69 reports, there remains no systematic analysis of the morphology of banding, the paleogeographic
70 distribution of banding or its relationship to hybrid-bed deposition. This fundamentally limits our

ability to use banding as a facies to characterize and interpret deep-water depositional environments.

The alternation of hydrodynamically different grain sizes within an individual deposit does not fit with established models of bedform development. Such conventional models derived from clean sand suspensions show that flow velocity and grain size are inter-dependent controls on bedform development (e.g. Southard and Boguchwal, 1990; Southard, 1991; Van den Berg and van Gelder, 1993). In these cases, flow turbulence segregates particles enabling the flow to deposit discrete grain size populations and diagnostic bedforms at different flow speeds (Baas et al., 2016). However, banding indicates that hydrodynamically distinct sand and mud grain-size populations are deposited under similar flow conditions in alternating layers. Two process models have been proposed to explain the origin of banding; bedform development under mud-rich transitional flows (Baas et al., 2011), and episodic near-bed turbulence damping (Lowe and Guy, 2000). The prominent model that interprets banding as a product of cyclic near-bed damping of turbulence and modulating flow behavior was derived from the subsurface Britannia Formation. In this model, periods of cleaner sand deposition alternate with mud-rich bands formed as near-bed shear disintegrates mud flocs and mud clasts resulting in increased cohesiveness and the development of a near-bed laminar plug (Lowe and Guy, 2000). Haughton et al. (2009) emphasize longitudinal flow transformation; whereby fine-grained cohesive particles are segregated towards the rear of the flow, which suppresses turbulence and generates a cohesive laminar plug. In this case, banding is interpreted to be generated beneath parts of the flow that are intermediate between turbulent and laminar (cohesive), as the flow transforms along its length. These models place banding within a narrow range of transitional flow conditions. However, recent experiments show that mixed sand/clay suspensions can modify conventional bedform stability zones and produce a variety of heterolithic deposits across a range of flow conditions (Baas et al., 2011, 2016; Schindler et al., 2015).

Outstanding questions in light of these advances include: Where does banding sit in relation to clean sand bedforms, what textural and morphological properties distinguish banding from conventional planar-laminated (T_b) sands, and what distribution does banding have in a turbidite facies tract?

We aim to document a range of banding textures and their facies associations from three ancient deep-water systems. Our objectives are to: i) describe and quantify the varied sedimentological character of banding, ii) place constraints on the spatial and stratigraphic distribution of banding, and iii) discuss the formational processes responsible for banding. Addressing these objectives permits us to present a model that links formational flow processes of banding with its stratigraphic and spatial distribution in order to improve process understanding and prediction of deep-water systems.

Terminology

Flow types

Herein, we use the term '*turbidity current*' to describe a flow that is non-cohesive and deposits sediment incrementally, which deposits a '*turbidite*' (Bouma, 1962). We distinguish between low-density flows that are dilute and turbulent, and high-density flows that have suppressed turbulence and support grains via hindered settling effects (Lowe, 1982). '*Debris flows*' are cohesive with sufficient clay content to suppress turbulence. They deposit *en masse* via frictional freezing to the bed, which produces a '*debrite*' (e.g. Iverson, 1997; Talling et al., 2012). Flows are capable of transformations between these turbulent and cohesive rheologies (Haughton et al., 2003; Felix and Peakall, 2006). This can produce a hybrid deposit comprising a genetically-linked turbidite-debrite

within a single event bed, which is called a '*linked-debrite*' (Wood and Smith, 1958; Haughton et al., 2003; Talling et al., 2012).

Laminae

Event beds contain divisions of sedimentary structures that are well-described in idealized facies sequences (e.g. Bouma, 1962; Lowe, 1982; Haughton et al., 2009; Talling et al., 2012). These divisions comprise structureless and laminated sandstones. '*Laminae*' are thin layers less than a centimeter thick that occur in discrete divisions within an event bed. Laminae are grain supported and have relatively sharp upper and lower boundaries, which denote a sharp change in grain size and/or sorting (Campbell, 1967; Arnott and Hand, 1989; Best and Bridge, 1992). As laminae become thicker (>5 mm) they tend to become more diffuse, whereby sorting values in the laminae are progressively similar to that of the surrounding sandstone (Sumner et al., 2008).

Mud and cohesivity

'Mud' is typically defined in the field as a mixture of clay, silt, and organic fragments, with potentially some very fine and fine sand (e.g. Winterwerp and van Kesteren, 2004; Kane et al., 2017). In terms of the grain-size of the solid components mud is defined as clay plus silt (McCave et al., 1995; Winterwerp and van Kesteren, 2004). The optical methodology used herein for the thin-section analysis has a lower resolution limit for grains of ~60 μm, thus the material below the resolution limit approximates to the <63 μm limit for 'mud'. Previous work on turbidites and linked-debrites has shown that the analysis of mud in thin-section supports the qualitative observations of mud in the field (Lowe and Guy, 2000; Kane et al., 2017; Bell et al., 2018a). A key question for the present work however is whether this <63 μm fraction is composed of detrital clay minerals and thus is indicative of deposition from cohesive flows. Whilst it is known that some silt-rich turbidites are

largely clay free (Strachan et al., 2016), we assume that the examples herein do contain detrital clay based on the following. Turbidites and linked debrites from the Karoo, South Africa, the field area for one of the examples herein, are known to contain between 10-35% clay, most of which is detrital in origin (Kane et al., 2017). More generally, mud typically contains a significant proportion of clay, particularly in deep-sea environments (Weaver, 1989; Winterwerp and van Kesteren, 2004; Stevenson et al., 2014; Dutkiewicz et al., 2015). Lastly, even silt-dominated turbidites typically contain appreciable (15-30%) clay (Piper, 1978; Stow and Piper, 1984) and exceptions are linked to a range of grading styles and structures (Strachan et al., 2016), which are not observed in the examples herein. We also recognise that inter-particle forces dictate that cohesive effects become important (i.e. influence flow rheology and settling dynamics) at grain sizes <30 μm (McAnally et al., 2007) whereby even quartz grains behave cohesively below 10 μm (McCave et al., 1995). Other materials such as organic fragments and extracellular polymeric substances, that are ubiquitous in deep-water environments, provide additional sources of cohesion in mud grain sizes (Craig et al., 2020). Hence, we assume that our thin section measurements of mud contain appreciable clay, and that the identification of mud in the sediments reflects cohesive forces in the flow from which they were deposited.

Definition of banding

Here, we use the term '*Banding*' to describe alternating light and dark layers within a single event bed. We distinguish between the alternating layers, and refer to dark, mud-rich layers as '*dirty bands*' and lighter, cleaner sandstone layers as '*cleaner bands*'. Individual dirty bands are mud-rich (as matrix and clasts), matrix supported, have very poor sorting, and are subdivided into mud-rich dirty bands and sand-rich dirty bands based on their mud content. Individual cleaner bands are grain supported, better sorted than dirty bands, and are subdivided into either mud-rich or sand-rich cleaner bands based on their mud content. Thin section analysis presented in this study quantifies

the mudstone content across these different categories of band. Our definition in this paper differs from previous work, where bands are recognized as couplets: a dark, mud-rich layer overlain by a light, cleaner sandstone layer (e.g. Lowe and Guy, 2000; Haughton et al., 2009). In this study, we demonstrate a variety of morphologies and contacts between dark, mud-rich layers and the lighter, cleaner sandstone layers, which does not support the couplet model. Hence, we redefine the definition of banding to accommodate these new insights.

MATRIALS AND METHODS

This study uses onshore borehole data and outcrops from the Karoo Basin, South Africa; offshore subsurface core data from the Magnus Oilfield, North Sea, UK, and outcrops in several localities in the Neuquén Basin, Argentina. Sedimentary successions in core and outcrop were logged at centimeter-scale. Twenty-five thin sections were made from selected deposits in core and outcrop, and were visually examined through a transmitted light optical microscope at 4× and 10× magnification. Point counting was conducted using a petrographic microscope with 300 points per slide to determine textural and compositional properties. Point counts were taken across several areas on each slide, which were focused along individual bands (areas ~1-5 × 10 mm), and within the cleaner sandstone divisions (areas ~5 × 10 mm). Grain-size was determined by measuring the maximum diameter of optically distinguishable grains. Following Bell et al. (2018a), the limit of optically resolvable grains was ~60 µm. Therefore, fine grains approximating to <63 µm are grouped together and termed ‘mud’. We first present each data set separately, as individual case studies, then summarize commonalities across the data sets.

Late Jurassic Magnus oilfield, North Sea

Geological Setting

The Late Jurassic Magnus oilfield sits on the northeastern margin of the Viking Graben; perched to the west of the Magnus-Penguin Basin in the North Sea (Fig. 2A). Accommodation developed in response to a series of Permo-Triassic to Late Jurassic North Sea rifting episodes (Dominguez, 2007), which influenced clastic depositional patterns across the oilfield (Fig. 2B) (Morris et al., 1999). The Magnus Sandstone Member (herein MSM) is an approximately 120 m thick sand-rich turbidite succession of Kimmeridgian age that is bounded above and below by the Kimmeridge Clay Formation (Fig. 2C). From core facies and biostratigraphic data, the MSM stratigraphy is divided into sub-units MSM-A through to MSM–G (Morris et al., 1999). An extensive core dataset from 27 wells has permitted the spatial extent and character of MSM stratigraphy across the oilfield to be constrained, which is interpreted in terms of three main depositional phases: (1) Late Kimmeridgian with a depocenter in the mid-field, sourced from the northwest and displaying laterally confined, fault-controlled channel-fill (MSM-A; Fig. 2B); (2) Early Volgian accretion of two depocenters forming either side of the N-S trending Brent High (MSM-B, through to MSM-E to the SW; Fig. 2B); and (3) Volgian as before but with the southward migration of the northern depocenter with fault confinement (MSM-G) (Ravnås and Steel, 1997; Morris et al., 1999).

This paper uses core M16, from the central part of the field (Fig. 2B), which contains the full stratigraphy described above. The interval examined here is MSM-C, a sand-rich turbidite succession which overlies MSM-B, a mud-rich mass transport deposit (Haughton et al., 2009; Figs 2C and 3) .

Results

The MSM-C interval is a sand-rich turbidite succession, approximately 5 m thick but laterally variable, which overlies an approximately 15 m thick mud-rich mass transport deposit (MSM-B). The MSM-C turbidite succession is finer-grained and less well sorted compared with the rest of the MSM

turbidite stratigraphy with almost every bed recording some form of mud-rich division (Fig. 3). Turbidites in this interval comprise thin- to medium-bedded (10-35 cm thick) fine-grained sandstones with erosive and non-erosive basal surfaces and weakly graded bed tops, overlain by a sharp grain-size break and a thin (2-5 cm) mud cap (Fig. 3). Banding occurs in a variety of positions in the beds including: a) throughout a bed; b) from the base to middle parts of a bed, overlain by clean planar-lamination and/or ripple cross-lamination; c) the middle parts of a bed, intercalated with clean planar-lamination, and; d) towards the top of the bed, overlying a structureless sandstone division.

Bands are parallel to sub-parallel, or can be low angle (5-9 degrees; measured relative to thin bedded heterolithic intervals with flat concordant bases) with thicknesses ranging from millimeters (Fig. 4A) up to 2 cm thick (Fig. 4B). Typically, dirty bands have sharp lower and upper contacts with cleaner bands commonly loaded into their upper parts (Fig. 4C). Dirty bands have an elevated proportion of mudstone as matrix and clasts (between 50-74%) compared to the surrounding cleaner bands (between 25-39%). Dirty bands are typically matrix-supported, but vary in the amount of sand they contain. Mud-rich dirty bands have isolated sand grains supported by the matrix (Fig. 4A, 4C). Sand-rich dirty bands have more sand grains, which tend to increase in abundance upwards within the dirty band and pass from matrix- to grain-supported (Fig. 4B). Although the proportion of sand grains may vary in the dirty bands, the maximum grain size is similar between dirty bands and cleaner bands. Both mud-rich and sand-rich dirty bands also contain a large amount of rounded sub-millimeter mudstone clasts, many of which are difficult to distinguish from the surrounding matrix mudstone (Fig. 4).

Paleogeographic setting

Regional correlation of the MSM stratigraphy from the Magnus oilfield shows that it extends for 5-10 km southeast into the Penguin Half Graben (Ravnås and Steel, 1997). Within the Magnus oilfield, the MSM succession is dominated by medium- to coarse-grained sandstones (Ravnås and Steel, 1997). Hence, the MSM succession at Magnus is interpreted to represent a relatively proximal paleoenvironment: a coarse-grained slope apron (Ravnås and Steel, 1997) or, drawing similarities from recent outcrop work, an intraslope lobe complex (Spychala et al., 2015).

Jurassic Los Molles Formation, Neuquén Basin, Argentina

Geological Setting

The Neuquén Basin is located in central-western Argentina and central eastern Chile, and extends up to 700 km in a north-south direction between latitude 32˚ S and 40˚ S (Fig. 5A). The basin is bounded by wide cratonic areas of the Sierra Pintada System, the North Patagonian Massif, and the Andean magmatic arc (Howell et al., 2005). During the Jurassic and Cretaceous, a post-rift back-arc basin developed (Vergani et al., 1995; Franzese and Spalletti, 2001; Franzese et al., 2003; Howell et al., 2005). The Lower-Middle Jurassic Cuyo Group represents the onset of marine deposition (Fig. 5B), comprising pelagic and hemipelagic mudstone intercalated with successions of sandstone turbidites: the Los Molles Formation (Gulisano and Gutiérrez Pleimling, 1995; Llambías et al., 2007; Paim et al., 2008) (Fig. 5C). This paper examines exhumed turbidites from the Los Molles Formation in the west-central sector of the Neuquén Basin at Location 1 about 15 km northeast of the town of Chos Malal, and Location 2 in the southern sector at La Jardinera, to the southeast of the town of Aluminé (Fig. 5).

Results

Chos Malal, Roadside Gully

Outcrop of the Los Molles Formation (UTM 0360472/5872607) shows across depositional strike exposures of banded sandstones over approximately 100 m with vertical exposures up to 2 m thick (Fig. 6). The base of the package comprises a chaotic mudstone with abundant angular clasts of mudstone and sandstone (Fig. 6A; below 1). This mudstone-rich facies is truncated by an erosion surface (Fig. 6A; 1), which is variably overlain by a mudstone-clast conglomerate (Fig. 6A; between 1 and 2), and medium-bedded (20-30 cm thick) amalgamated banded sandstones (Fig. 6A; between 2 and 3). The succession is capped by a thick (1-2 meters) gravel conglomerate (Fig. 6A; above 3). Dirty bands within the amalgamated sandstone are sub-parallel to wavy and discontinuous with sharp bases and tops. They are either: i) thin (millimeters) primarily composed of small (mm diameter) mudstone-clasts (Fig. 6B), or ii) thick (centimeters) bands composed of very small mudstone clasts (sub-mm diameter) with an increased proportion of matrix mud compared to the surrounding cleaner bands (Fig. 6C and 6D). Dirty bands have variable mudstone clast content with lateral grading from mudstone clast conglomerate facies (Fig. 6A), to zones of banded sandstone composed of abundant mudstone clasts, and banded zones with a relatively low proportion of mudstone (Fig. 6E). These banded divisions with low mudstone content can have weakly developed lamination within the cleaner bands (Fig. 6E). Typically, bands are sub-parallel to wavy and clustered into 3-10 cm thick divisions showing pinch-and-swell morphologies over meters. They occur towards bed tops, overlying structureless sandstone (Figs 6C and 6D).

Chos Malal, Roadside Cutting

Exposure of the Los Molles Formation (UTM 365568.08/5874549.43) at a similar stratigraphic interval several kilometers down dip of the roadside gully outcrop shows amalgamated banded

sandstones (Fig. 7A). Here, beds comprise an erosional basal surface that is overlain by banded sandstone. Where amalgamation is less pronounced, banded sandstones are overlain by a sharp grain-size break and a relatively thin mudstone cap. The basal parts of beds can be marked by a mudstone clast conglomerate lag or a structureless sandstone division. The banding is initially cleaner and becomes more dirty upwards (Fig. 7B and 7C). Bands are sub-parallel in the lower parts of the bed, which pass upwards into more complex heterolithic bedforms (Fig. 7B). Sub-parallel dirty bands pinch and swell, and can be discontinuous over decimeters to meters (Fig. 7C facies B_{PS} and B_{PM}). In contrast, the heterolithic bedforms are low-angle (5-7 degrees) with wavelengths between 15-30 cm (Fig. 7C facies B_{CL}). The low-angle bedforms grade upwards into shorter wavelength ripple-like heterolithic bedforms with more consistently steeply dipping foresets (10 degrees) (Fig. 7C facies B_{CR}).

La Jardinera, Road Cutting

The La Jardinera outcrop (UTM: 0349119/5638150) is exposed along a road cutting and shows the strike architecture of a succession of thin- to medium-bedded (5-40 cm thick) medium-grained sandstones (Fig. 8A). The succession is characterized by stacked structureless sandstone beds with banded tops, or less-commonly banded bases. The basal structureless and banded sandstone divisions are sharply overlain by a grain-size break and a thin mudstone cap (Figs 8B, 8C, 8D and 8E). Thicker beds (30-40 cm thick) within the central part of the succession are bounded below by a meter-thick interval of fine-grained thin beds, and above by another fine-grained thin-bedded interval (poor exposure) and turbidites with linked-debrites (Fig. 8B). Linked-debrite bed divisions found in the upper part of the succession contain weakly deformed elongate intraformational clasts of banded sandstone, approximately 40 cm long and 10 cm thick (Fig. 8C). Sandstone beds are generally ungraded but locally have coarser bases and normally graded tops. Banded divisions are laterally variable in thickness (2-10 cm) over meters with sub-parallel bands pinching and swelling,

and commonly pinching out over meters (Figs 8D and 8E). Individual dirty bands have sharp upper and lower contacts, are typically millimeters to centimeters thick, and are composed primarily of mudstone clasts (Figs 9A). Mudstone clasts are sub-millimeter up to 1 cm in diameter, rounded and elongate, poorly sorted with some clasts aligned with their long-axis sub-parallel to the dirty band (Figs 9B and 9C). Individual dirty bands can have a uniform abundance of mudstone clasts throughout (Fig. 9A), or show a progressive upward increase (Fig. 9B) or decrease (Fig. 9C) in the amount of mudstone clasts through the dirty band. The overall proportion of mudstone (including matrix and clasts) within the dirty bands is elevated (between 51-66%) compared to the surrounding cleaner bands (between 32-40%).

Paleogeographic Setting

The Los Molles Formation comprises marine pelagic and hemipelagic mudstones, punctuated by sandy turbidites (Gulisano and Gutiérrez Pleimling, 1995; Llambías et al., 2007; Paim et al., 2008). The Chos Malal succession preserves banded sandstones with coarse beds of gravel and thick (1-2 meters) conglomerates (Figs 6A and 7A). The association of marine mudstones with very coarse gravity flow deposits indicates this is a proximal setting: likely a lower slope or base of slope environment. The La Jardinera succession preserves amalgamated packages of medium-grained, thick-bedded sandstones that are separated by thinner-bedded heterolithic packages (Fig. 8B). Towards the top of the logged section, linked debrites occur in association with a thin-bedded heterolithic package. This is typical of compensational lobe stacking, whereby thick-bedded amalgamated sandstones represent lobe axes and thinner-bedded sandstone with linked-debrites representing lobe off-axis to lobe frontal fringe environments (Prélat et al., 2009; Spychala et al., 2017). The coarse-grained nature of the sandstones coupled with compensational lobe stacking suggests La Jardinera represents a relatively proximal lobe setting, either an intraslope or base of slope environment.

Late Permian Skoorsteenberg Formation, Karoo Basin, South Africa

Geological Setting

The Karoo Basin is interpreted to have developed in the Permian through subsidence in response to subduction (Tankard et al., 2009) prior to developing as a retroarc foreland basin during the Early Mesozoic (Johnson, 1991; Cole, 1992; Visser, 1993). The Laingsburg depocenter in the southwest Karoo Basin consists of deep-water fill represented by the lower Ecca Group, specifically the Vischkuil, Laingsburg and Fort Brown formations (Fig. 10). These three formations comprise a 2 km thick shallowing-upward succession from distal basin-floor through continental slope to shelf-edge and deltaic settings (Fig. 10) (Wickens, 1994; Flint et al., 2011). This paper uses outcrop in the Laingsburg depocenter. The Laingsburg Formation is divided into Units A and B (Sixsmith et al., 2004; Brunt et al., 2013) (Fig. 10). Unit A is 350 m thick, comprising seven sandstone-prone sub-units (A1-A7), which are separated by regionally extensive mudstones. Here, we examine an outcrop in the Geelbeck River area within sub-unit A5 (Fig. 10).

Results

Laingsburg, Geelbek River, Unit A5

In general, sub-unit A5 in the Geelbek River is characterized by thick bedded fine-grained sandstones with low relief scours (Fig. 11A). Variable incision and amalgamation by overlying beds is common. Where amalgamation is less pronounced, sandstone divisions are sharply overlain by a grain-size break and a thin mudstone cap. Lenticular mudstone-clast lags typically overlie erosion surfaces (Sixsmith et al., 2004). Banding occurs in a variety of positions in beds with either erosive or non-erosive bases; most commonly towards the top of fine-grained structureless sandstone beds (Fig.

11A). However, it also occurs towards the base of beds overlain by parallel laminated sandstone, or within the middle parts of beds, between basal structureless sandstone and overlying planar laminated sandstone. Dirty bands comprise large amounts of small (millimeter diameter) rounded mudstone clasts, and an increased proportion of mudstone within the matrix. Dirty bands are millimeters to centimeters thick and have sharp upper and lower contacts with cleaner bands, which are commonly loaded into the upper contact with the dirty band. Banding is present in a variety of morphologies: sub-parallel and low-angle (4-9 degrees) bands that pinch-and-swell over meters downstream (Fig. 11B), and more complex heterolithic bedforms (Fig. 11C). Figure 11C shows a complex heterolithic bedform where the upstream (left side) of the bedform has relatively steeply dipping (16 degrees), weakly climbing foresets with alternations of cleaner sandstone and dirty bands. These foresets transition downstream (over decimeters to meters) into low-angle (5 degrees) to sub-parallel banding (low-amplitude bedwaves). Thicknesses of cleaner and dirty bands vary across the bedform.

Paleogeographic setting:

The Geelbeck area is interpreted to be situated on the proximal basin-floor (close to base-of-slope) and close to distributive basin-floor channels within the axis of deposition of sub-unit A5 (Sixsmith et al., 2004).

Summary of characteristics of banding in turbidite sandstones

Banding appears as 5-35 cm thick divisions of alternating light and dark bands within turbidite sandstones. Bands typically occur within fine to very-fine grained sandstones (Figs 3, 6, 7 and 11) but can also occur in coarser sandstone (Fig. 8). These banded divisions can occur in a variety of bed positions, including towards the base, middle and upper parts (Figs 3, 6, 8 and 11), and can be

384 developed throughout a bed (Figs 3 and 7B). Banding can be found at the base, overlying an erosive
385 or non-erosive surface, whilst banding that occurs in the middle to upper parts of beds typically
386 overlies a basal structureless sandstone division (Figs 3, 6C, 8E, 11A) and/or a mudstone clast
387 conglomerate lag (Fig. 7A). Furthermore, banding can also be found intercalated with clean planar
388 laminated sands. Banding is commonly overlain by planar-laminated sandstone (Figs 4A and 7C), and
389 in some cases by ripple cross-lamination. Sandstone beds are typically amalgamated but where
390 amalgamation is less pronounced, banded sandstones are overlain by a grain-size break and a thin
391 mudstone cap. Dirty bands are intercalated with cleaner bands containing planar- and low-angle
392 laminae (Figs 4 and 7C, 11B). Banding forms a variety of morphologies and is laterally variable: sub-
393 parallel to low angle bands that pinch-and-swell over 1-3 meters (Figs 3, 7, 8, 11B) that may grade
394 laterally into mudstone clast conglomerate facies (Figs 6A and 6C); more complex heterolithic
395 bedforms with a mix of more steeply dipping foresets that transition downstream into decimeter-
396 wavelength low-angle bedwaves (Fig. 11C); or ripple-scale banded bedforms recording discontinuous
397 lenses of mudstone over 15-30 cm wavelengths (Fig. 7C; B_{CL} and B_{CR}). Individual beds can show an
398 upwards progression from sub-parallel banding into low-angle complex heterolithic banding, which
399 in turn transitions into shorter wavelength more steeply dipping heterolithic banding (Fig. 7C). In
400 terms of paleoenvironment, banding is generally found in proximal localities: base-of-slope channel
401 mouth settings of the Geelbek River, South Africa (Fig. 10) (Sixsmith et al., 2004; Hofstra et al., 2015),
402 and relatively proximal slope settings in the Magnus oilfield (Fig. 2) (Ravnås and Steel, 1997; Ravnås
403 et al., 2000), Chos Malal (Figs 6 and 7) and La Jardinera outcrops (Fig. 8). Commonly, banding occurs
404 in successions immediately overlying mud-rich substrates, where the beds have erosional basal
405 surfaces and contain an abundance of intraformational mudstone clasts (Figs 3 and 6A).

406 Bands generally have sharp upper and lower contacts with cleaner bands loading into dirty bands.
407 Dirty bands have an elevated proportion of mudstone as matrix and clasts (total mudstone content
408 typically 45-75%) compared to the cleaner bands (typically 25-45%; Figs 4 and 9), although there is a
409 continuum from sand-rich cleaner bands (~25-35%) through mud-rich cleaner bands (~35-45%) and

sand-rich dirty bands (~45-55%) to mud-rich dirty bands (~55-75%) (Fig. 12). Mudstone clasts within individual dirty bands are sub-millimeter to 1 cm in diameter, rounded and elongate (Fig. 9). Their abundance can be uniform, or decrease or increase upwards within an individual dirty band (Fig. 9). The mudstone clasts are most likely a combination of recycled lithic mudstones (often several millimeters in diameter and rounded) and softer muds eroded from the seafloor during the flow's passage. These softer mud clasts exhibit a range of diameters but tend to be sub-millimeter, irregularly shaped, and are often observed wrapped around grains or larger examples forming cm-scale tendril-like shapes within the sandstones. The proportion of sand within a dirty band can vary from a mud-rich dirty band with isolated floating sand grains to a sand-rich dirty band with a higher proportion of sand (Fig. 12), and can increase in the amount of sand upwards and become grain-supported at its top (Figs 4 and 6). Mud-rich dirty bands contain >55% mudstone, are matrix-supported, and provide evidence for cohesive strength such as sheared fabrics and isolated floating sand grains (e.g. Figs 4A and 4C). Sand-rich dirty bands are also matrix-supported but have a lower mudstone content of ~45-55% and have an increased proportion of poorly sorted sand grains within the bands (e.g. Figs 4B and 9A). They still retain features of poor grain segregation and shearing, indicating deposition from a flow with cohesive strength (Iverson, 1997). Mud-rich cleaner bands contain ~35-45% mudstone and are grain supported (e.g. Figs 4B and 6E). Finally, sand-rich cleaner bands contain <35% mudstone, are grain supported and are better sorted than mud-rich cleaner bands (Fig. 12). Sorting of grains is evidence of grain-by-grain deposition and traction beneath a turbulent flow (Allen, 1982; Best and Bridge, 1992; Sumner et al., 2008). Identification of the continuum of mud content from sand-rich cleaner bands to mud-rich dirty bands can be difficult to distinguish visually, and thus banding is likely more prevalent than currently recognised.

DISCUSSION

Origins of banding

435 Banding comprises alternating mud-rich (dark) and cleaner sandstone (light) layers within a single
436 event bed. We recognize that the proportion of clay contained within the mud-rich layers is not
437 directly constrained by the point count measurements. However, as discussed earlier (see 'Mud and
438 cohesivity' section), we assume that the mud in the samples herein contains appreciable clay and
439 that elevated mud content reflects cohesive forces in the parent flows. Therefore, existing models
440 that interpret deposits as a product of cohesionless flows are not appropriate to interpret banded
441 sandstones, including: Low-Density Turbidites (Bouma, 1962), High-Density Turbidites (Lowe, 1982),
442 and Near-Bed Grain Flows (Mutti, 1992). Indeed, such models do not describe or attempt to
443 interpret heterolithic sedimentary structures. Currently, there are two competing process models
444 proposed to explain the origin of banding in sandstones; episodic near-bed turbulence damping
445 (Lowe and Guy, 2000), and bedform development under mud-rich transitional flows (Baas et al.,
446 2011, 2016).

447

448 *Episodic near-bed turbulence damping*

449 Lowe and Guy (2000) proposed that banding develops at the base of flows that vary between
450 turbulent and laminar states, through the cyclic development of near-bed cohesive plugs. These
451 plugs are postulated to form through episodic near-bed turbulence damping through electrical
452 charge induced bonding of clays, following disaggregation of clay flocs (Lowe and Guy, 2000). This
453 hypothesis was initially based on banded sandstones from the Lower Cretaceous Britannia
454 Formation, North Sea, which comprise sub-parallel mud-rich (matrix supported) bands that range in
455 thickness from a few millimeters (microbanding) through to >50 cm (megabanding) (Guy, 1992;
456 Blackbourn and Thomson, 2000; Lowe and Guy, 2000; Lowe et al., 2003; Barker et al., 2008; Fig. 1).
457 Banded sandstone divisions in this field can be up to several meters thick, and occur overlying clean
458 structureless sandstone. In the Britannia Formation examples, banding passes upwards into either a
459 clean planar-laminated sandstone, or more commonly into a mud-rich linked-debrite. Individual

460 bands are matrix-supported with clean sandstone loaded into their upper contacts and abundant
461 syn-sedimentary dewatering features, such as sheared and truncated pipes. The presence of thick
462 mega- and macro- bands with pervasive dewatering structures provides evidence for rapid
463 deposition. Later work on banding within hybrid beds has incorporated this process model and
464 linked it to longitudinal flow transformation, specifically a period between dominantly cohesionless
465 flow depositing high-density turbidites and more cohesive flow producing mud-rich sandstones and
466 debrites (Davis et al., 2009; Haughton et al., 2009; Southern et al., 2017). In this hybrid bed model, a
467 relatively thin (1-15 cm) banded sandstone occurs between a clean basal turbidite sandstone and an
468 overlying mud-rich linked-debrite within a single event bed. Individual bands are sub-parallel and
469 exhibit a sheared matrix- and loaded upper contacts. Bands may grade upwards from thicker,
470 muddier bands into thinner bands containing predominantly carbonaceous material (Davis et al.,
471 2009).

472

473 *Bedforms under mud-rich transitional flows*

474 In contrast to the concept of cyclical freezing of a near-bed plug, experimental work under
475 transitional flows (*sensu* Baas et al., 2009) with well-developed cohesive plugs has demonstrated
476 that banded deposits can form within the upper stage plane bed flow regime, and the washed out
477 ripple regime (transitional zone between true ripples and upper stage plane beds), via the migration
478 of bedforms over a period of >2 hours (Fig. 13) (Baas et al., 2011, 2016). Transitional plug flows form
479 through the presence of cohesive clay within a flow, which progressively modifies turbulence (from
480 enhanced to damped) as clay content increases. This results in the development of a laminar plug,
481 which grows downward from an interval of low shear stress (Baas et al., 2009). This transitional flow
482 behavior is governed by the balance of turbulent versus cohesive forces (Baas et al., 2009, 2011,
483 2016). Lower Transitional Plug Flows (*sensu* Baas et al., 2009) produced sub-parallel bands of muddy
484 sand overlain by low amplitude bedwaves comprising isolated streaks of clayey sand (Baas et al.,

2016). Over time, shallow scouring and the downstream migration of the bedwaves generated complex asymmetric heterolithic stratification: steeply dipping lenses of cohesive clay foresets, overlain by low-amplitude clayey sand bedwaves, which in turn were partially overlain by cleaner-sand low-amplitude bedwaves. Upper Transitional Plug Flows (*sensu* Baas et al., 2009) produced sub-parallel bands of sandy clay, which were overlain by heterolithic low-angle cross-laminated sand or parallel-laminated cleaner sand (Baas et al., 2016). There have been indications from field observations that banding can exhibit wavy morphologies (Hofstra et al., 2015, 2018). However, there has been no field evidence for the presence of bedwaves, and low-angle and steeply dipping foresets, which would support the experimental observations.

Field evidence

The examples of banding reported in this study are characterized by divisions 5-35 cm thick, composed of individual bands that are millimeters to 2 cm thick. They occur in a variety of bed positions and have a range of different morphologies including sub-parallel and low-angle, and bedforms comprising both sub-parallel bands juxtaposed with low-angle and steeply dipping bands. In addition, the mud content of individual dirty bands varies from matrix-supported mud-rich dirty bands through to dirty bands with a higher proportion of sand grains (Fig. 12). Additionally, banding reported in this study does not have strong syn-sedimentary dewatering features, such as sheared pipe and dish structures. Rather, banding in this study shows more subtle loading structures (Fig. 4C). The morphologies and sedimentological characteristics of the banded sandstones documented in our field data have similar characteristics to the thin and sharp heterolithic laminae produced in the experiments of Baas et al. (2016) (Fig. 13). Examples of these similarities include the complex asymmetrical heterolithic stratification in the Geelbek River (Fig. 11C); low-angle banding in the Magnus core (Fig. 4A); and sub-parallel banding in La Jardinera (Fig. 8). Given the variety in morphology, bed position and mud content observed in our examples, they are interpreted to be

510 the product of deposition (and reworking) from transitional flows with a sustained period of
511 traction, which have well-developed laminar plugs (Figs. 13 and 14; Baas et al., 2016). The clear
512 evidence for traction in many of these examples, through bedwaves and low- and steeply-dipping
513 foresets is incompatible with cyclic instantaneous freezing of a near bed plug flow, given that this
514 would allow no time for tractional movement. Hence, we interpret banding in these examples as the
515 product of tractional bedforms under sustained transitional flows (*sensu* Baas et al., 2009). Although
516 we did not observe strong dewatering structures (pipes and dishes) in the field examples, the
517 experiments of Baas et al. (2016) do report small-scale fluid-escape features in the more rapidly
518 aggraded deposits.

519

520 **Rate of flow deceleration**

521 In addition to the balance of cohesive versus turbulent forces, experiments with mixed sand/clay
522 suspensions show that the rate of flow deceleration fundamentally influences deposit character (Fig.
523 14). This is because deceleration is a primary control on aggradation rate, which governs the amount
524 of time the bed is exposed to traction (shear) from the overriding flow (e.g. Allen, 1982; Southard
525 and Boguchwal, 1990; Vrolijik and Southard, 1997; Leclair and Arnott, 2005; Sumner et al., 2008).
526 Rapidly decelerated cohesive suspensions (high clay content) produce debrite and linked-debrite
527 deposits without banding (Sumner et al., 2009; Baas et al., 2011). Cohesive flows that are
528 decelerated comparatively slowly generate sub-parallel banding (Baas et al., 2016). Less cohesive
529 flows (reduced clay content) at these longer deceleration times are able to produce more complex
530 banded sands (heterolithic bedforms of Baas et al., 2011, 2016). With even longer deceleration
531 times, near-bed turbulence (even in cohesive flows) has time to winnow the bed of fines, which
532 promotes segregation of clay/sand and results in largely clean laminated sand overlain by clay
533 (Malarkey et al., 2015; Baas et al., 2016) (Fig. 14).

534

535 **Multiple depositional models for banding?**

536 As interpreted here, banding can develop as bedforms beneath progressively aggrading transitional
537 flows (Baas et al., 2016). This mechanism is associated with relatively thin (millimeters to
538 centimeters) bands, which have a variety of bedform morphologies, and do not display strong syn-
539 sedimentary dewatering features (pipes and dishes); albeit experiments suggest some small-scale
540 dewatering features may be present (Baas et al., 2016). The exact character of the bands is governed
541 by the flow state: the balance of cohesive versus turbulent forces, and the rate of flow deceleration.
542 However, this tractional bedform mechanism may not be an explanation for the relatively thick (> 50
543 cm), matrix-supported, sub-parallel bands containing abundant syn-sedimentary dewatering
544 features, which characterize facies such as those in the Britannia Formation (Lowe and Guy, 2000)
545 and Springar Formation (Southern et al., 2017). Such sediments have largely been examined via core,
546 and there has not yet been evidence for cross-lamination (cross-stratification) and thus for traction
547 at the base of the flow. Furthermore, it seems unlikely that segregation of particles via traction
548 under a flow could generate such thick bands. Consequently, the postulated model for banding in
549 these systems, that they are produced via the cyclic deposition and rapid aggradation of near-bed
550 cohesive plugs (Lowe and Guy, 2000), remains the most plausible. Therefore, it appears that there
551 are two separate formative mechanisms for banding within deep-marine clastic sediments.

552

553 The transition between more fluidal flows and highly mud-rich debris flows, as is thought to occur in
554 hybrid beds (Haughton et al., 2009), will be dominated by transitional clay-rich flows (*sensu* Baas et
555 al., 2009). Considering the evidence presented herein that such flows are likely to produce banding
556 via tractional bedforms, given the correct transitional flow regime and deceleration profile, then it
557 would appear far more likely that such a mechanism is responsible for banding in hybrid beds, than

558 the Lowe and Guy (2000) model of cyclic freezing of near-bed plugs. This tractional-model for
559 banding in hybrid beds was first postulated by Baas et al. (2011), and the present work provides very
560 strong support for the importance of transitional flows (*sensu* Baas et al., 2009) in the formation of
561 hybrid bed banding.

562

563 ***T_b, or not T_b?***

564 Here, we have demonstrated that the field examples of banding are tractional bedforms and that
565 they are highly analogous to the transitional flow experiments of Baas et al. (2016) from the upper
566 stage plane bed (USPB) and washed out ripple (WOR) flow regime. Non-cohesive flows depositing in
567 the same regimes are associated with planar-lamination (Bouma T_b division) and low-amplitude
568 ripples (Bouma T_b/T_c division boundary), respectively. Banding in the examples herein occupies a
569 similar position within a vertical facies succession as clean parallel-lamination. It occurs: i) towards
570 the top of beds overlying structureless sandstone, ii) as a basal division overlain by parallel-
571 laminated sandstone and/or ripples, iii) in the middle parts of beds sandwiched between basal
572 structureless sandstone and overlying parallel-laminated sandstone, or iv) is intercalated with clean
573 planar-laminated sandstone. As banding occupies similar flow regimes as parallel-lamination (i.e.
574 USPB and WOR) and occurs at a similar positions within vertical facies successions as T_b parallel-
575 laminated sandstones, it suggests that banding represents the T_b division for clay-rich transitional
576 flows, with moderate rates of deceleration (see section on Rate of flow deceleration). Given this
577 conclusion, we suggest that the Bouma T_b clean sandstone division and banding may occupy a
578 similar position along a turbidite facies tract. However, the spatial relationship between banded
579 bedforms and true T_b lamination is made complicated by the nature of flow transformation from
580 turbulent to cohesive transitional flow states; this evolution can in turn be related to a facies tract.
581 We explore this concept below.

582

583 **Distribution of Banded Sandstones and Linked-Debrites**

584 Here, we use examples of banded sandstones and linked-debrites from the literature alongside
585 insights gained from this study to propose a conceptual distribution of these facies across deep-
586 water systems (Fig. 15). This study recognizes banding within intraslope basins (Figs 2 and 3; Fig. 15A
587 Part i), base-of-slope channel mouth settings (Fig. 10; Fig. 15A Part ii), and less well-constrained
588 proximal slope settings (Figs 6 and 7). Previous work has also associated banding with proximal
589 settings (Barker et al., 2008; Kane and Pontén, 2012; Southern et al., 2017), and specific deep water
590 environments including: channel splays (Fig. 15A Part iii) and immediately overlying mud-rich MTD's
591 (Davis et al., 2009); immediately down-dip of channel-mouth scours (Hofstra et al., 2015), and at
592 base-of-slope lobes (Fig. 15A Part ii) (Spychala et al., 2017; Hofstra et al., 2018). In contrast, banded
593 sandstones in distal settings are rarely reported. Instead, linked-debrites without an intermediary
594 banded division are common (Fig. 15A Part iv), comprising clean basal sandstone directly overlain by
595 mud-rich chaotic sandstone (Talling et al., 2004, 2007; Amy and Talling, 2006; Davis et al., 2009;
596 Haughton et al., 2009; Lee et al., 2013; Talling, 2013; Fonnesu et al., 2015, 2018; Spychala et al.,
597 2017; Mueller et al., 2017). Where banded sandstones occur in distal fan fringe settings, they are
598 relatively thin divisions (up to 15 cm) sandwiched between the clean basal sandstone and the
599 overlying mud-rich linked-debrite (Haughton et al., 2009). Confining slopes may also influence the
600 distribution of banded sandstones and linked-debrites (Fig. 15A Part v). Examples of both banded
601 sandstones and linked-debrites have been associated individually with mud-draped confining
602 topography (Barker et al., 2008; Patacci et al., 2014; Southern et al., 2017; Bell et al., 2018b). Indeed,
603 if confinement is pervasive along the length of a deep-water system then banded sandstones may be
604 expected in more distal settings, such as documented in the Springar Formation, North Sea
605 (Southern et al., 2017).

606

A model for banding in submarine fans

Given that banding and hybrid beds are both linked to cohesive, clay-rich flows, why is it that banded sandstones are rarely part of the same hybrid bed and are associated with different deep water environments? We propose that the rate of deceleration in transitional flows, along with the balance of cohesive versus turbulent forces, controls the distribution of banded sandstones and linked-debrites (Figs 14, 15B and 15C). In relatively proximal locations, flows are likely to be quasi-steady with a sustained period of velocity and low rates of deceleration, whilst in more distal settings flows are more likely to be unsteady and subject to rapid deceleration via catastrophic collapse of flow turbulence (Fig. 15B) (Kane et al., 2009, 2017; Stevenson et al., 2014). Proximal quasi-steady transitional flows will produce periods of sustained traction, which promotes the development of a variety of banded bedforms (Fig. 15C). Their exact morphology will depend on the cohesive strength of the flow, the near-bed turbulence, and the amount of time the bed is reworked (Fig. 14). Rapid flow deceleration in distal settings results in rapid aggradation and the suppression of traction. Without sustained traction, banded bedforms are not able to develop. Instead, when cohesive forces dominate over flow turbulence, a thick cohesive plug develops, which deposits *en masse* as a debrite (Fig. 15C). This idealized distribution can be perturbed. Flows that entrain large volumes of mud and/or exceptionally cohesive mud in proximal localities can transform rapidly into cohesive flows, which locally deposit linked-debrites within 100's of meters down dip of the site of erosion (Fig. 15C) (Fonnesu et al., 2015, 2018; Southern et al., 2015; Brooks et al., 2018). Confining slopes may force local changes in rates of flow deceleration, resulting in the deposition of either linked-debrites (Patacci et al., 2014; Bell et al., 2018b) or banded sandstones (Southern et al., 2017).

Recognition criteria for banding

630 Banding in the field or in core is recognized as alternating dark (dirty) and lighter (cleaner) layers
631 occurring within a single event bed. Bands have an elevated proportion of mud compared to the
632 surrounding cleaner sandstone divisions ranging from grain-supported sand-rich cleaner bands (>25-
633 45% mud content) through to matrix supported mud-rich dirty bands (45-75% mud content). These
634 are similar to average mud contents reported from banded sandstones in the Britannia field (18-
635 30%), with dirty bands potentially having twice the amount of mud compared to the cleaner bands
636 (Lowe and Guy, 2000). Key differences between banding and T_b parallel-laminated sandstones are: i)
637 an elevated proportion of mud (25-75%; this study) compared to clean planar-laminated sandstone
638 (5-10%; Sylvester and Lowe, 2004; Stevenson et al., 2014); ii) the dirty bands are matrix supported in
639 contrast to grain-supported layers in T_b; iii) cleaner and dirty bands both exhibit poor sorting within
640 bands, unlike T_b which is well sorted within individual laminae; iv) banding comprises alternating
641 layers with each band demarcated by a sharp change in mud content whilst T_b exhibits abrupt
642 changes in sorting between laminae (Allen, 1982; Best and Bridge 1992; Sumner et al., 2008); v) dirty
643 bands may have a sheared matrix and commonly exhibit small-scale dewatering features, such as
644 loading of cleaner bands into dirty bands, whereas deformation is absent in T_b, and, vi) the
645 morphology of bands includes low-amplitude bedwaves punctuated by steeply dipping heterolithic
646 foresets, and shorter wavelength higher-amplitude ripple-like heterolithic structures, in addition to
647 sub-parallel layers similar in shape to T_b parallel-lamination. Despite these criteria, the range of
648 lower mud contents in banded sandstones can in some cases make it difficult to distinguish banding
649 visually from clean T_b parallel-laminated sandstone in outcrop and core, and thus banding is likely to
650 be under recognized.

651 Recognition criteria for differentiating between banding formed by traction under transitional flows
652 as described herein, as against those formed by episodic near-bed turbulence damping (Lowe and
653 Guy, 2000) are: i) the close relationship between banding and Bouma T_b in vertical facies successions
654 for transitional flows; ii) spatial variations in morphology (e.g., discontinuous down-dip; low-angled
655 bedforms; bedwaves; steeply dipping foresets) present in transitional flows whilst turbulence-

damped banding is always sub-parallel; iii) macrobanding (10-50 cm thick) and megabanding (>50 cm thick) are solely associated with episodic turbulence damping, as these are too thick to form under traction; and, iv) pervasive syn-sedimentary dewatering structures such as sheared and truncated pipes are associated with turbulence damping, reflecting far more rapid deposition than under tractional regimes. Whilst, the morphological criterion is only applicable in outcrop, the other criteria can be utilized in both field and core.

CONCLUSIONS

We examine banding within turbidite sandstones using a suite of outcrop and core data from three different deep-water systems: the Lower Jurassic, Magnus Oilfield, North Sea; the Lower Jurassic Neuquén Basin, Argentina, and the Permian Karoo Basin, South Africa. Bands are recorded in very fine- to medium-grained sandstones in a variety of bed positions including base, middle and top. Banding occurs above, erosive and non-erosive basal surfaces, mudstone lags, or structureless sands, and is overlain by clean parallel-laminated sandstones and/or ripple cross-lamination. Banded divisions may also be intercalated with planar lamination. Individual dirty bands are relatively thin (mm to cm) and have an elevated proportion of mudstone (between 45-75% as matrix and clasts) compared to intercalated cleaner bands (between 25-45%), although a continuum of mud content is recognized from sand-rich through to mud-rich cleaner bands, and sand-rich to mud-rich dirty bands. Banded divisions range in thickness (5-30 cm), mud content and morphology (from sub-parallel to composite heterolithic bedforms). Banded sandstones occur in proximal settings that are situated close to sites of erosion into muddy substrates. This style of banding is interpreted to comprise a range of bedforms that form progressively within, and at the boundaries of, the upper stage plane bed regime via tractional reworking beneath mud-laden transitional plug flows. The conditions under which banding can develop are similar to those of planar-laminated (T_b) sandstone, the primary difference being an elevated proportion of cohesive mud within the flow. The balance of

cohesive versus turbulent forces, and the rate of flow deceleration (aggradation rate) govern the style of deposit. Banded sandstones and linked-debrites rarely overlie each other within the same bed, and are associated with proximal and distal deep-water environments respectively. The rate of flow deceleration is key to explaining this distribution, whereby in proximal settings, slow rates of deceleration subject the bed to a period of traction (producing banding), whilst in distal settings flows rapidly decelerate resulting in minimal traction (producing debrites). This model of banding in the T_b flow regime is in marked contrast to earlier work invoking cyclic aggradation of near-bed cohesive plugs, although such plugs provide an explanation for much thicker bands that lack evidence of traction, suggesting that banding can be polygenetic. Understanding the origins of banding and the conditions under which it is formed, its distribution across deep-water systems, and its relationship to linked-debrites, is important for it to be used effectively as a tool to interpret the geological record.

Acknowledgements

CS and DH thank BP for funding work on the Magnus system. JP is very grateful to the UK Natural Environment Research Council for grant NE/C514823/1 (TransFlow), which allowed the underpinning work on bed development under mixed sand-mud flows to be undertaken. The contributions of AP and DB were supported by the LOBE 2 joint industry consortium research project, which was funded by Anadarko, Bayerngas Norge, BG Group, BHP, BP, Chevron, Dong Energy, Engie, Premier Oil, Maersk Oil, Marathon Oil, Petrobras, Shell, Statoil, Total, VNG Norge and Woodside. The British Geological Survey (BGS) is thanked for access to and sampling of Magnus cores. Menno Hofstra is gratefully acknowledged for the pictures of the complex heterolithic bedforms and initial sedimentary log shown in Figure 11. Esther Sumner, Lorna Strachan, and Editor Katherine Maier are thanked for their thorough and constructive reviews, which greatly improved the paper.

705

706 **References**

707

708 Allen, J.R.L., 1982. Sedimentary structures: their character and physical basis, Volume 1. Amsterdam,
709 Elsevier.

710 Amy, L.A., Talling, P.J., 2006. Anatomy of turbidites and linked debrites based on long distance (120 x
711 30 km) bed correlation, Marnoso Arenacea Formation, Northern Apennines, Italy.
712 Sedimentology, v. 53, p. 161–212. doi:10.1111/j.1365-3091.2005.00756.x

713 Arnott, R.W.C., Hand, B.M., 1989. Bedforms, primary structures and grain fabric in the presence of
714 suspended sediment rain. Journal of Sedimentary Petrology, v. 59, p. 1062–1069.

715 Baas, J.H., Best, J.L., Peakall, J., 2016. Predicting bedforms and primary current stratification in
716 cohesive mixtures of mud and sand. Journal of the Geological Society of London, v. 173, p. 12–
717 45. doi:10.1144/jgs2015-024.

718 Baas, J.H., Best, J.L., Peakall, J., 2011. Depositional processes, bedform development and hybrid bed
719 formation in rapidly decelerated cohesive (mud-sand) sediment flows. Sedimentology, v. 58, p.
720 1953–1987. doi:10.1111/j.1365-3091.2011.01247.x

721 Baas, J.H., Best, J.L., Peakall, J., Wang, M., 2009. A phase diagram for turbulent, transitional, and
722 laminar clay suspension flows. Journal of Sedimentary Research, v. 79, p. 162–183.
723 doi:10.2110/jsr.2009.025.

724 Barker, S.P., Haughton, P.D.W., McCaffrey, W.D., Archer, S.G., Hakes, B., 2008. Development of
725 rheological heterogeneity in clay-rich high-density turbidity currents: Aptian Britannia
726 Sandstone Member, UK continental shelf. Journal of Sedimentary Research, v. 78, p. 45–68.
727 doi:10.2110/jsr.2008.014.

728 Bell, D., Kane, I.A., Pontén, A.S.M., Flint, S.S., Hodgson, D.M., Barrett, B.J., 2018a. Spatial variability in
729 depositional reservoir quality of deep-water channel-fill and lobe deposits. Marine and
730 Petroleum Geology, v. 98, p. 97–115. https://doi.org/10.1016/j.marpetgeo.2018.07.023

731 Bell, D., Stevenson, C.J., Kane, I.A., Hodgson, D.M., Poyatos-Moré, M., 2018b. Topographic controls
732 on the development of contemporaneous but contrasting basin-floor depositional
733 architectures. Journal of Sedimentary Research, v. 88, p. 1166–1189. doi:10.2110/jsr.2018.58.

734 Best, J., Bridge, J., 1992. The morphology and dynamics of low amplitude bedwaves upon upper
735 stage plane beds and the preservation of planar laminae. Sedimentology, v. 39, p. 737–752.

736 Blackbourn, G.A., Thomson, M.E., 2000. Britannia Field, UK North Sea: petrographic constraints on
737 Lower Cretaceous provenance, facies and the origin of slurry-flow deposits. Petroleum
738 Geoscience, v. 6, p. 329–343. doi:10.1144/petgeo.6.4.329.

739 Bouma, A.H., 1962. Sedimentology of some Flysch Deposits: A Graphic Approach to Facies
740 Interpretation. Elsevier, Amsterdam/New York, 168 pp.

741 Brooks, H.L., Hodgson, D.M., Brunt, R.L., Peakall, J., Hofstra, M., Flint, S.S., 2018. Deep-water
742 channel-lobe transition zone dynamics: Processes and depositional architecture, an example
743 from the Karoo Basin, South Africa. Geological Society of America Bulliten, v. 130, p. 1723–
744 1746. doi:10.1130/B31714.1.

745 Brunt, R.L., Hodgson, D.M., Flint, S.S., Pringle, J.K., Di Celma, C., Prelat, A., Grecula, M., 2013.
746 Confined to unconfined: Anatomy of a base of slope succession, Karoo Basin, South Africa.
747 Marine and Petroleum Geology, v. 41, p. 206–221. doi:10.1016/j.marpetgeo.2012.02.007.

748 Campbell, C.V., 1967. Lamina, laminaset, bed and bedset. Sedimentology, v. 8, p. 7–26.
749 doi:10.1111/j.1365-3091.1967.tb01301.x

750 Cole, D., 1992. Evolution and development of the Karoo Basin. *in* Witt, M.J. Ransome, I.G.D., eds.,

751 Inversion Tectonics of Capre Fold Belt, Karoo and Cretaceous Basins of South Africa: Balkema,
752 Amsterdam, p. 87–99.

753 Craig, M.J., Baas, J.H., Amos, K.J., Strachan, L.J., Manning, A.J., Paterson, D.M., Baker, M.L., 2020.
754 Biomediation of submarine sediment gravity flow dynamics. Geology, v. 48(1), p. 72–76.
755 https://doi.org/10.1130/G46837.1

756 Davis, C., Haughton, P., McCaffrey, W., Scott, E., Hogg, N., Kitching, D., 2009. Character and
757 distribution of hybrid sediment gravity flow deposits from the outer Forties Fan, Palaeocene
758 Central North Sea, UKCS. Marine and Petroleum Geology, v. 26, p. 1919–1939.
759 doi:10.1016/j.marpetgeo.2009.02.015.

760 Dominguez, R., 2007. Structural evolution of the Penguins Cluster, UK northern North Sea, *in* Jolley,
761 S.J., Barr, D., Walsh, J.J., Knipe, R.J., eds., Structurally Complex Reservoirs: Geological Society
762 Publishing House, Bath, pp. 25–48. doi:10.1144/sp292.2.

763 Dutkiewicz, A., Müller, R.D., O'Callaghan, S. and Jónasson, H., 2015. Census of seafloor sediments in
764 the world's ocean. Geology, 43, 795-798.

765 Felix, M. and Peakall, J., 2006. Transformation of debris flows into turbidity currents: mechanisms
766 inferred from laboratory experiments. Sedimentology, v. 53, p. 107-123.

767 Flint, S.S., Hodgson, D.M., Sprague, A.R., Brunt, R.L., van der Merwe, W.C., Figueiredo, J., Prelat, A.,
768 Box, D., Di Celma, C., Kavanagh, J.P., 2011. Depositional architecture and sequence stratigraphy
769 of the Karoo basin floor to shelf edge succession, Laingsburg depocentre, South Africa. Marine
770 and Petroleum Geology, v. 28, p. 658–674. doi:10.1016/j.marpetgeo.2010.06.008.

771 Fonnesu, M., Felletti, F., Haughton, P.D.W., Patacci, M., McCaffrey, W.D., 2018. Hybrid event bed
772 character and distribution linked to turbidite system sub-environments: The North Apennine
773 Gottero Sandstone (north-west Italy). Sedimentology, v. 65, p. 151-190,

doi:10.1111/sed.12376.

Fonnesu, M., Haughton, P., Felletti, F., McCaffrey, W., 2015. Short length-scale variability of hybrid event beds and its applied significance. Marine and Petroleum Geology, v. 67, p. 583–603. doi:10.1016/j.marpetgeo.2015.03.028

Franzese, J., Spalletti, L., Perez, I.G., Macdonald, D., 2003. Tectonic and paleoenvironmental evolution of Mesozoic sedimentary basins along the Andean foothills of Argentina (32 degrees-54 degrees S). Journal of South American Earth Sciences, v. 16, p. 81–90. doi:10.1016/s0895-9811(03)00020-8.

Franzese, J.R., Spalletti, L.A., 2001. Late Triassic-early Jurassic continental extension in southwestern Gondwana: tectonic segmentation and pre-break-up rifting. Journal of South American Earth Sciences, v. 14, p. 257–270. doi:10.1016/s0895-9811(01)00029-3.

Gulisano, C.A., Gutiérrez Pleimling, A.R., 1995. The Jurassic of the Neuquén Basin. *in* Neuquén Province: Buenos Aires, Asociación Geológica Argentina Field Guide, Serie E2, 111 p.

Guy, M., 1992. Facies analysis of the Kopervik sand interval, Kilda Field, Block 16/26, UK North Sea, *in* Hardman, R.F.P., eds., Exploration Britian: Geological insights for the next Decade. Geological Society of London Special Publication, v. 67, p. 187–220.

Haughton, P.D.W., Barker, S.P., McCaffrey, W.D., 2003. “Linked” debrites in sand-rich turbidite systems - origin and significance. Sedimentology, v. 50(3), p. 459–482.

Haughton, P., Davis, C., McCaffrey, W., Barker, S., 2009. Hybrid sediment gravity flow deposits - Classification, origin and significance. Marine and Petroleum Geology, v. 26, p. 1900–1918. doi:10.1016/j.marpetgeo.2009.02.012.

Hofstra, M., Hodgson, D.M., Peakall, J., Flint, S.S., 2015. Giant scour-fills in ancient channel-lobe transition zones: Formative processes and depositional architecture. Sedimentary Geology, v.

329, p. 98–114. doi:10.1016/j.sedgeo.2015.09.004.

Hofstra, M., Peakall, J., Hodgson, D.M., Stevenson, C.J., 2018. Architecture and morphodynamics of subcritical sediment waves in an ancient channel-lobe transition zone. Sedimentology, v. 65, p. 2339–2367. doi:10.1111/sed.12468.

Howell, J.A., Schwarz, E., Spalletti, L.A., Veiga, G.D., 2005. The Neuquen Basin: an overview. *in* Veiga, G.D., Spalletti, L.A., Howell, J.A., Schwarz, E., eds., Neuquen Basin, Argentina: A Case Study in Sequence Stratigraphy and Basin Dynamics. Geological Society Publishing House, Bath, p. 1–14. doi:10.1144/gsl.sp.2005.252.01.01.

Iverson, R.M., 1997. The physics of debris flows. Reviews of Geophysics, v. 35, p. 245–296.

Johnson, M.R., 1991. Sandstone petrography, provenance and plate tectonic setting in Gondwana context of the southeastern Cape-Karoo Basin. South African Journal of Geology, v. 94, p. 137–154.

Kane, I.A., McCaffrey, W.D., Martinsen, O.J., 2009. Allogenic vs. autogenic controls on megaflute formation. Journal of Sedimentary Research, v. 79, p. 643–651. doi:10.2110/jsr.2009.072.

Kane, I.A., Pontén, A.S.M., 2012. Submarine transitional flow deposits in the Paleogene Gulf of Mexico. Geology, v. 40, p. 1119–1122. doi:10.1130/g33410.1.

Kane, I.A., Pontén, A.S.M., Vangdal, B., Eggenhuisen, J.T., Hodgson, D.M., Spychala, Y.T., 2017. The stratigraphic record and processes of turbidity current transformation across deep-marine lobes. Sedimentology, v. 64, p. 1236–1273. doi:10.1111/sed.12346.

Leclair, S.F., Arnott, R.W.C., 2005. Parallel lamination formed by high-density turbidity currents. Journal of Sedimentary Research, v. 75, p. 1–5. doi:10.2110/jsr.2005.001.

Lee, S.H., Jung, W.Y., Bahk, J.J., Gardner, J.M., Kim, J.K., Lee, S.H., 2013. Depositional features of co-genetic turbidite-debrite beds and possible mechanisms for their formation in distal lobated

bodies beyond the base-of-slope, Ulleung Basin, East Sea (Japan Sea). Marine Geology, v. 346, p. 124–140. doi:10.1016/j.margeo.2013.09.001.

Llambías, E.J., Leanza, H.A., Carbone, O., 2007. Evolución Tectono-magmática durante el pérmico al Jurásico temprano en la Cordillera del Viento (37°05□S - 37°15□S): Nuevas evidencias geológicas y geoquímicas Del Inicio de la Cuencas Neuquina. Revista de la Asociación Geológica Argentina, v. 62, p. 217–235.

Lowe, D.R., 1982. Sediment gravity flows .2. Depositional models with special reference to the deposits of high-density turbidity currents. Journal of Sedimentary Petrology, v. 52, p. 279–298.

Lowe, D.R., Guy, M., 2000. Slurry-flow deposits in the Britannia Formation (Lower Cretaceous), North Sea: a new perspective on the turbidity current and debris flow problem. Sedimentology, v. 47, p. 31–70. doi:10.1046/j.1365-3091.2000.00276.x

Lowe, D.R., Guy, M., Palfrey, A., 2003. Facies of slurry-flow deposits, Britannia Formation (Lower Cretaceous), North Sea: implications for flow evolution and deposit geometry. Sedimentology, v. 50, p. 45–80.

McCave, I.N., Manighetti, B., Robinson, S.G., 1995. Sortable silt and fine sediment size/composition slicing: Parameters for palaeocurrent speed and palaeoceanography. Paleoceanography, v. 10(3), p. 593–610. https://doi.org/10.1029/94PA03039

McAnally, W.H., Friedrichs, C., Hamilton, D., Hayter, E., Shrestha, P., Rodriguez, H., Teeter, A., 2007. Management of fluid mud in estuaries, bays, and lakes. I: Present state of understanding on character and behavior. Journal of Hydraulic Engineering, v. 133(1), p. 9–22. https://doi.org/10.1061/(ASCE)0733-9429(2007)133:1(9)

Malarkey, J., Baas, J.H., Hope, J.A., Aspden, R.J., Parsons, D.R., Peakall, J., Paterson, D.M., Schindler, R.J., Ye, L., Lichtman, I.D., Bass, S.J., Davies, A.G., Manning, A.J., Thorne, P.D., 2015. The

843 pervasive role of biological cohesion in bedform development. Nature Communications, v. 6,
844 6257. doi:10.1038/ncomms7257.

845 Morris, P.H., Payne, S.N.J., Richards, D.P.J., 1999. Micropalaeontological biostratigraphy of the
846 Magnus Sandstone Member (Kimmeridgian-Early Volgian), Magnus Field, UK North Sea. *in*
847 Jones, R.W., Simmons, M.D., eds., Biostratigraphy in Production and Development Geology, v.
848 152, p. 55–73. doi:10.1144/gsl.sp.1999.152.01.04.

849 Mueller, P., Patacci, M., Di Giulio, A., 2017. Hybrid event beds in the proximal to distal extensive lobe
850 domain of the coarse-grained and sand-rich Bordighera turbidite system (NW Italy). Marine and
851 Petroleum Geology, v. 86, p. 908–931. doi:10.1016/J.MARPETGEO.2017.06.047.

852 Paim, P.S.G., Silveira, A.S., Lavina, E.L.C., Faccini, U.F., Leanza, H.A., Teixeira De Oliveira, J.M.M.,
853 D'Avila, R.S.F., 2008. High resolution stratigraphy and gravity flow deposits in the Los Molles
854 Formation (Cuyo Group - Jurassic) at La Jardinera region, Neuquén basin. Revista de la
855 Asociación Geológica Argentina, v. 63, p. 728–753.

856 Patacci, M., Haughton, P.D.W., McCaffrey, W.D., 2014. Rheological complexity in sediment gravity
857 flows forced to decelerate against a confining slope, Braux, SE France. Journal of Sedimentary
858 Research, v. 84, p. 270–277. doi:10.2110/jsr.2014.26.

859 Pierce, C.S., Haughton, P.D.W., Shannon, P.M., Pulham, A.J., Barker, S.P., Martinsen, O.J., 2018.
860 Variable character and diverse origin of hybrid event beds in a sandy submarine fan system,
861 Pennsylvanian Ross Sandstone Formation, western Ireland. Sedimentology, v. 65, p. 952–992.
862 doi:10.1111/sed.12412.

863 Piper, D.J.W., 1978. Turbidite muds and silts on deepsea fans and abyssal plains. In: Sedimentation in
864 Submarine Canyons, Fans and Trenches (Eds D.J.Stanley and G.Kelling), pp. 163–176. Dowden,
865 Hutchinson and Ross, Stroudsburg, PA.

866 Prélat, A., Hodgson, D.M., Flint, S.S., 2009. Evolution, architecture and hierarchy of distributary
867 deep-water deposits: a high-resolution outcrop investigation from the Permian Karoo Basin,
868 South Africa. Sedimentology, v. 56, p. 2132-U25. doi:10.1111/j.1365-3091.2009.01073.x

869 Ravnås, R., Nøttvedt, A., Steel, R.J., Windelstad, J., 2000. Syn-rift sedimentary architectures in the
870 Northern North Sea, *in* Nøttvedt, A., eds., Dynamics of the Norwegein Margin, Geological
871 Society of London Special Publication, v. 167, p. 133–177. doi:10.1144/GSL.SP.2000.167.01.07.

872 Ravnås, R., Steel, R.J., 1997. Contrasting styles of Late Jurassic syn-rift turbidite sedimentation: A
873 comparative study of the Magnus and Oseberg areas, northern North Sea. Marine and
874 Petroleum Geology, v. 14, p. 417–449. doi:10.1016/s0264-8172(97)00010-x.

875 Schindler, R.J., Parsons, D.R., Ye, L., Hope, J.A., Baas, J.H., Peakall, J., Manning, A.J., Aspden, R.J.,
876 Malarkey, J., Simmons, S., Paterson, D.M., Lichtman, I.D., Davies, A.G., Thorne, P.D., Bass, S.J.,
877 2015. Sticky stuff: Redefining bedform prediction in modern and ancient environments.
878 Geology, v. 43, p. 399–402. doi:10.1130/g36262.1

879 Sixsmith, P.J., Flint, S.S., Wickens, H.D., Johnson, S.D., 2004. Anatomy and stratigraphic development
880 of a basin floor turbidite system in the Laingsburg Formation, main Karoo Basin, South Africa.
881 Journal of Sedimentary Research, v. 74, p. 239–254. doi:10.1306/082903740239.

882 Southard, J.B., 1991. Experimental determination of bedform stability. Annual Review of Earth and
883 Planetary Sciences, v. 19, p. 423–455. doi:10.1146/annurev.earth.19.1.423.

884 Southard, J.B., Boguchwal, L.A., 1990. Bed configurations in steady unidirectional water flows. 2.
885 Synthesis of flume data. Journal of Sedimentary Petrology, v. 60, p. 658–679.

886 Southern, S.J., Kane, I.A., Warchoł, M.J., Porten, K.W., McCaffrey, W.D., 2017. Hybrid event beds
887 dominated by transitional-flow facies: character, distribution and significance in the
888 Maastrichtian Springar Formation, north-west Vøring Basin, Norwegian Sea. Sedimentology, v.

64, p. 747–776. doi:10.1111/sed.12323.

Southern, S.J., Patacci, M., Felletti, F., McCaffrey, W.D., 2015. Influence of flow containment and substrate entrainment upon sandy hybrid event beds containing a co-genetic mud-clast-rich division. Sedimentary Geology, v. 321, p. 105–122. doi:10.1016/j.sedgeo.2015.03.006.

Spychala, Y.T., Hodgson, D.M., Flint, S.S., Mountney, N.P., 2015. Constraining the sedimentology and stratigraphy of submarine intraslope lobe deposits using exhumed examples from the Karoo Basin, South Africa. Sedimentary Geology, v. 322, p. 67–81. doi:10.1016/j.sedgeo.2015.03.013.

Spychala, Y.T., Hodgson, D.M., Prélat, A., Kane, I.A., Flint, S.S., Mountney, N.P., 2017. Frontal and lateral submarine lobe fringes: Comparing sedimentary facies, architecture and flow processes. Journal of Sedimentary Research, v. 87, p. 75–96. doi:10.2110/jsr.2017.2

Stevenson, C.J., Talling, P.J., Masson, D.G., Sumner, E.J., Frenz, M., Wynn, R.B., 2014. The spatial and temporal distribution of grain-size breaks in turbidites. Sedimentology, v. 61, p. 1120–1156. doi:10.1111/sed.12091.

Stow, D.A.V, Piper, D.J.W., 1984. Deep-water fine-grained sediments: facies models. In: Fine-Grained Sediments: Deep-Water Processes and Facies. (Eds Stow, D.A.V. and Piper, D.J.W.) The Geological Society, 15, p. 611–646.

Strachan, L.J., Bostock, H.C., Barnes, P.M., Neil, H.L., Gosling, M., 2016. Non-cohesive silt turbidity current flow processes; insights from proximal sandy-silt and silty-sand turbidites, Fiordland, New Zealand. Sedimentary Geology, v. 342, p. 118–132. https://doi.org/10.1016/j.sedgeo.2016.06.017Sumner, E.J., Amy, L.A., Talling, P.J., 2008. Deposit structure and processes of sand deposition from decelerating sediment suspensions. Journal of Sedimentary Research, v. 78, p. 529–547. doi:10.2110/jsr.2008.062.

Sumner, E.J., Talling, P.J., Amy, L.A., 2009. Deposits of flows transitional between turbidity current

and debris flow. Geology, v. 37, p. 991–994. doi:10.1130/g30059a.1

Sylvester, Z., Lowe, D.R., 2004. Textural trends in turbidites and slurry beds from the Oligocene flysch of the East Carpathians, Romania. Sedimentology, v. 51, p. 945–972. doi:10.1111/j.1365-3091.2004.00653.x

Talling, P.J., 2013. Hybrid submarine flows comprising turbidity current and cohesive debris flow: Deposits, theoretical and experimental analyses, and generalized models. Geosphere, v. 9, p. 460–488. doi:10.1130/ges00793.1

Talling, P.J., Amy, L.A., Wynn, R.B., Peakall, J., Robinson, M., 2004. Beds comprising debrite sandwiched within co-genetic turbidite: origin and widespread occurrence in distal depositional environments. Sedimentology, v. 51, p. 163–194. doi:10.1046/j.1365-3091.2003.00617.x

Talling, P.J., Masson, D.G., Sumner, E.J., Malgesini, G., 2012. Subaqueous sediment density flows: Depositional processes and deposit types. Sedimentology, v. 59, p. 1937–2003. doi:10.1111/j.1365-3091.2012.01353.x

Talling, P.J., Wynn, R.B., Masson, D.G., Frenz, M., Cronin, B.T., Schiebel, R., Akhmetzhanov, A.M., Dallmeier-Tiessen, S., Benetti, S., Weaver, P.P.E., Georgiopoulou, A., Zuhlsdorff, C., Amy, L.A., 2007. Onset of submarine debris flow deposition far from original giant landslide. Nature, v. 450, p. 541–544. doi:10.1038/nature06313.

Tankard, A., Welsink, H., Aukes, P., Newton, R., Stettler, E., 2009. Tectonic evolution of the Cape and Karoo basins of South Africa. Marine and Petroleum Geology, v. 26, p. 1379–1412. doi:http://dx.doi.org/10.1016/j.marpetgeo.2009.01.022

Van den Berg, H.H., van Gelder, A., 1993. A new bedform stability diagram with emphasis on the transition of ripples to plane bed in flows over fine sand and silt. *in* Marzo, M. and Puigdefabregas, C., eds., Alluvial Sedimentation: International Association of Sedimentologists

Special Publications, v. 17, p. 11–21.

Vergani, G.D., Tankard, A.J., Belotti, H.J., Welsink, H.J., 1995. Tectonic evolution and paleogeography of the Neuquén Basin, Argentina. *in* Tankard, A.J., Suarez, S. Welsink, H.J., eds., Petroleum Basins of South America: American Association of Petroleum Geologists Memoir, v. 62, p. 383–402.

Visser, J.N.J., 1993. Sea-level changes in a back-arc-foreland transition: the late Carboniferous-Permian Karoo Basin of South Africa. Sedimentary Geology, v. 83, p. 115–131. doi:http://dx.doi.org/10.1016/0037-0738(93)90185-8.

Vrolijik, P.J., Southard, J.B., 1997. Experiments on rapid deposition of sand from high-velocity flows. Geoscience Canada, v. 24, p. 45–54.

Weaver, C.E., 1989. Clays, muds and shales. Elsevier, Developments in Sedimentology, 44, Amsterdam.

Wickens, H. de V, 1994. Basin floor fan building turbidites of the southwestern Karoo Basin, Permain Ecca Group, South Africa [PhD Thesis]. University of Port Elizabeth.

Winterwerp, J.C., W.G.M. van Kesteren, 2004. Introduction to the Physics of Cohesive Sediments in the Marine Environment, Developments in Sedimentology, 56, Elsevier, New York, 466 pp.

Wood, A., Smith, A.J., 1958. The sedimentation and sedimentary history of the Aberystwyth Grits (Upper Llandoverian). Quarterly Journal of the Geological Society, v. 114, p. 163–195.

Figure captions

Figure 1. Cartoon logs with example core photos illustrating banded sandstone facies and hybrid beds documented from the Britannia and Springar formations (1-4) and the Paleogene Forties Fan, North Sea (5-6). Britannia and Springar banding (top left) occurs in exceptionally thick divisions several meters thick with individual bands several centimeters thick (up to >50 cm thick) associated with abundant dewatering pipes. Core photos, upper center, show thick macrobanding (dark brown) transitioning upwards into thinner mesobanding (light brown). Megabanding is shown on the right hand side. Arrows highlight individual dirty bands (modified from Lowe and Guy, 2000; their Fig. 10). Banding in the Forties Fan is included within the idealized hybrid bed model of Haughton et al. (2009), whereby it occurs as a decimeter thick division sandwiched between a clean basal sandstone and an overlying linked-debrite (bottom left). Individual bands are typically several centimeters thick. The lowermost core photo shows banding within a hybrid bed within the Everest field, well section depth 8569-8564 ft (modified after Haughton et al., 2009; their Fig. 6). Note that banded divisions can be sand-prone or argillaceous in character. The key refers also to Figures 3, 5, 6, 7, 8, 11 and 14. Banding is represented as mudstone stripes (grey), however this covers dirty bands with a variety of different sandstone contents. References: 1) Lowe and Guy (2000), 2) Lowe et al. (2003), 3) Barker et al. (2008), 4) Southern et al. (2017), 5) Haughton et al. (2009), and 6) Davis et al. (2009).

Figure 2. Geological setting of the Magnus oilfield. (A) The Magnus oilfield is situated in the NW margin of the Viking Graben between the Møre Basin, and the Magnus-Penguin Basin to the SE. (B) Core locations and major structures across the Magnus oilfield (note M16 is core used in this study). Magnus Sandstone Member (MSM) depocenters are marked for MSM-A (fault controlled channel sandstones through the central part of the field); MSM-B (field-wide MTD that also covers MSM-A), and; MSM-C and E (with a lobe-like depocenter to the SE) adapted from Morris et al. (1999). (C) Stratigraphy of the Magnus oilfield comprises a sandstone-rich turbidite interval called the Magnus Sandstone Member (MSM), which is bounded above and below by the mud-rich intervals of the

Upper and Lower Kimmeridge Clay formations, respectively. The interval examined in this paper is within the lower part of the MSM succession.

Figure 3. Sedimentary log from the upper part of MSM-B (mud-rich mass transport deposit), through MSM-C (muddy turbidites) and into MSM-E (clean turbidites). The spatial distribution of these intervals across the field is shown in Figure 2B. Note the MSM-C turbidites are dirty compared to the overlying MSM-E turbidite stratigraphy with almost all beds recording some form of mud-rich banding (see Fig. 1 for key). Banding occurs in a variety of positions in the beds. Details of selected beds are shown in Figure 4.

Figure 4. Details of banded facies within the Magnus MSM-C turbidites. Dirty bands are composed of a large amount of rounded sub-millimeter diameter mudstone clasts and an elevated proportion of matrix. (A) Thin sub-parallel mud-rich dirty bands containing isolated floating sand grains, which are intercalated with cleaner bands composed of planar-laminated sandstone. (B) Thicker bands with sharp mud-rich bases grading upwards into cleaner bands, which founder down into the muddier underlying band. (C) Thin sub-parallel, low-angle and wavy mud-rich bands with isolated floating sand grains. Dirty bands have loaded upper contacts with the overlying cleaner bands. BGS sample numbers for thin sections: (A) SSK54784 (B) SSK54786 (C) SSK54787.

Figure 5. Geological setting of the Neuquén Basin. (A) Showing the extent of the Neuquén Basin, bounded on each side by orogenies. Outcrops used to examine banded sandstones are situated near the towns of Chos Malal (1) and Aluminé (2), marked with red stars on the GoogleEarth™ inserts. (B) Stratigraphic context of the sections presented in this study, which sit within the Early/Middle Jurassic Los Molles Formation. (C) Stratigraphy through the Los Molles Formation, showing deep-

1005 marine mudstones (black) punctuated by sandy turbidite deposition (yellow), coarse gravels and
1006 conglomerate deposits (orange), and mass transport deposits (green) (after Gulisano and Gutiérrez
1007 Pleimling, 1995; Llambías et al., 2007). See Fig. 1 for key. Studied sections (red stars) are described in
1008 more detail in Figs 6, 7 and 8.

1009

1010 **Figure 6.** Chos Malal Roadside Gully (see Fig. 5 for stratigraphic position). (A) Outcrop showing an
1011 erosion surface (red dashed line) (marked 1) cutting into a chaotic mud-rich sandstone, which is
1012 overlain by mud clast conglomerate (between 1 and 2) that grades laterally into thinner mudstone
1013 clast horizons. In turn, this is overlain by amalgamated banded sandstone beds (between 2 and 3).
1014 The banded sandstone is overlain by a clast supported gravel bed (marked 3) containing intra- and
1015 extra-formational mudstone and sandstone clasts (see Fig. 1 for key). (B) Close up of bands in Part A,
1016 showing they are discontinuous and composed of small elongated mud clasts. (C) Shows outcrop 100
1017 m across strike from Part A with the erosion surface (1), overlain by amalgamated banded
1018 sandstones (inferred bed contact shown as red dashed line), and the gravel bed (3). Banded divisions
1019 are variable in thickness laterally, occur towards the tops of beds and become more mud-rich
1020 upwards. Note that the lowermost banded sandstones are laterally equivalent to the mud-clast
1021 conglomerate in Part A. (D) Individual bands vary in thickness laterally, are sub-parallel to very low-
1022 angle and composed of a large amount of mudstone clasts. (E) Thin section of a zone of banded
1023 sandstone with a relatively low proportion of total mudstone (plane polarised light left, and cross-
1024 polarised light right). Note the weakly developed cleaner bands with occasional mudstone clasts
1025 (white dashed lines). Lens cap in A, C and D is 7 cm diameter. White arrows highlight banded
1026 sandstone divisions or individual dirty bands (Parts C and D respectively).

1027

Figure 7. Chos Malal Roadside Cutting (see Fig. 5 for stratigraphic position). Turbidite sandstones with distinct styles of banding. (A) Sedimentary log of Part B, showing amalgamated banded beds with erosional bases and mud clast conglomerate lags (see Fig. 1 for key). (B) Beds have lateral and vertical heterogeneity in facies with lenticular mud clast conglomerate lags and variable styles of banding. (C) Progression of banding styles upwards within an individual bed. At the base is a sand-prone division with sub-parallel bands (B_{PS}) that pinch and swell over decimeters and are commonly discontinuous. This is sharply overlain by (B_{PM}) a mud-prone division with slightly thicker (up to 1 cm) sub-parallel dirty bands and separated by thinner cleaner bands. In turn, this is sharply overlain by (B_{CL}) that is composed of complex low-angle heterolithic banding with bands forming lenses over 10-15 cm. This low-angle banding grades upwards into more steeply dipping ripple-like mud-rich bedforms (B_{CR}). Lens cap is 7 cm diameter.

Figure 8. La Jardinera Road Cutting Outcrop. (A) Outcrop showing the across strike architecture of a succession of thin to medium-bedded sandstones. Flow direction into page. (B) Sedimentary log of outcrop in Part A (see Fig. 1 for key) with supporting photographs showing: (C) a linked-debrite with mudstone and banded sandstone clasts, (D) a sub-parallel banded sandstone division at the top of a bed with significant lateral variation in the amount of mudstone clasts, (E) a sub-parallel banded division overlying a structureless sandstone, and (F) relatively thin bedded sub-parallel banded sandstones. Bed bases (red dashed lines) and internal bed facies divisions (white dashed lines) are marked. White arrows highlight banded divisions. Lens cap is 7 cm diameter.

Figure 9. Thin sections taken from La Jardinera road cutting outcrop (see Figs 8D and 8F for location of samples). (A) Thin section from a banded interval overlying a thin bedded sandstone, showing dirty bands composed of a large amount of small-diameter mudstone clasts and an elevated

proportion of matrix mudstone compared to the cleaner bands. Cleaner bands are loaded into the upper contacts of the mud-rich bands. Note that the bands are sub-parallel to low angle with thickness variations seen over centimeters. (B) Laterally equivalent section over meters to Part A, showing scattered mud clasts within a poorly sorted cleaner sandstone with an increasing abundance of mudstone clasts upwards into a dirty band. (C) Thin section across the boundary between a dirty band, composed primarily of rounded mudstone clasts that decrease in abundance upwards, and an overlying cleaner band with much better sorting and occasional sub-millimeter mudstone clasts.

Figure 10. Geological setting of the Laingsburg depocenter, Karoo Basin, South Africa. Top left showing stratigraphy and interpretation of paleoenvironments (after Flint et al., 2011), and bottom right the paleo-reconstruction of the fan environment (based on Sixsmith et al., 2004; Hofstra et al., 2015). The Geelbek outcrop is situated in a relatively proximal basin-floor to base-of-slope setting within the axis of deposition of Unit A5, and close to channels.

Figure 11. (A) Sand-prone succession of thin to medium bedded sandstones within Unit 4 of the Lainsburg depocenter, Geelbek River, Karoo Basin (see Fig. 1 for key). Banding typically occurs towards bed tops and presents a variety of morphologies. (B) Sub-parallel dirty bands intercalated with cleaner bands showing faint planar lamination. (C) A complex heterolithic bedform comprising steeply dipping muddy foresets on the left, which transition downstream into low-amplitude sandstone and mudstone bedwaves. White arrows highlight dirty bands. Lens cap 7 cm diameter.

Figure 12. Proportion of total mud content (matrix and mudstone clasts) versus detrital grain content within individual bands. Nq are samples from the Neuquén Basin and Mg are samples from

the Magnus oilfield. The yellow circle shows mudstone contents in a dirty band described from the Carpathian Flysch (Sylvester and Lowe, 2004). Note the range of mud content in both dirty and cleaner bands from mud-rich to sand-rich dirty bands, and the continuum into mud-rich and sand-rich cleaner bands.

Figure 13. Comparison of banded sandstone from the field (this study; Figs 4B and 11C) with mixed mud/sand stratification from the experiments of Baas et al. (2016). Note the similarities between heterolithic banding in the field and mixed sand/mud stratification in the experiments. Variations in banding morphology are likely linked with flow velocity and the balance of turbulent versus cohesive forces near to the bed (see main text for more detail). Flow regimes shown are Washed Out Ripples (WOR) and Upper Stage Plane Bed (USPB).

Figure 14. Conceptual phase space showing how deposit character changes with the cohesive strength of the flow (mud content) and rate of flow deceleration (linked to rate of aggradation). In addition, with increasing cohesive strength flows will decelerate more rapidly, ultimately depositing en masse. Example deposits are sourced from experiments on mixed sand/mud suspensions: 1) Sumner et al. (2009), 2) Baas et al. (2011), 3) Baas et al. (2016) and, 4) field deposits from this study. D_b = mud-rich debrite. L-D_b = linked-debrite. ST = clean structureless sandstone. B_P = sub-parallel banding (e.g. Fig. 4B). B_{CL} = low-angle complex heterolithic banding (e.g. Fig. 11C). B_{CR} = higher-angle complex banding at ripple-scale (e.g. Fig. 7C). PL = planar lamination. RXL = rippled cross-laminated sand. Note that linked-debrites and banded sands are produced from flows with relatively high cohesive strength (i.e. high mud content). However, banded sandstones require slower deceleration rates (a prolonged period of traction) to form than linked debrites.

Figure 15. (A) Conceptual model of the distribution of clean turbidite sandstone, banded sandstone and linked-debrites across a deep-water clastic system. Banded sandstones are postulated to be relatively proximal facies found close to sites of erosion into muddy substrates: (i) early intraslope lobes, (ii) immediately down dip of channel mouth scours and proximal lobe settings, and (iii) channel splays. (iv) Linked-debrites are a relatively distal facies associated with distal and lateral lobe fringes. (v) Flows interacting with basin topography can produce banded sandstones and linked-debrites local to the base of confining slopes. (B) Interpreted steadiness of flows at proximal and distal locations (adapted from Kane et al., 2009; Stevenson et al., 2014). Proximally, rate of flow deceleration is slow with a period of traction at the bed, which promotes deposition of banded sandstones. Distally, flow deceleration is rapid and deposits are emplaced en-masse with minimal traction, resulting in deposition of linked-debrites. (C) Conceptual facies tract produced by transitional flows showing the evolution of deposits from the site of mud entrainment (adapted from Kane et al., 2017; Fonnesu et al., 2017). Flows entrain mud and become mixed cohesive/turbulent suspensions. The balance of cohesive versus turbulent forces and rate of flow deceleration governs the style of deposition (see main text for details).

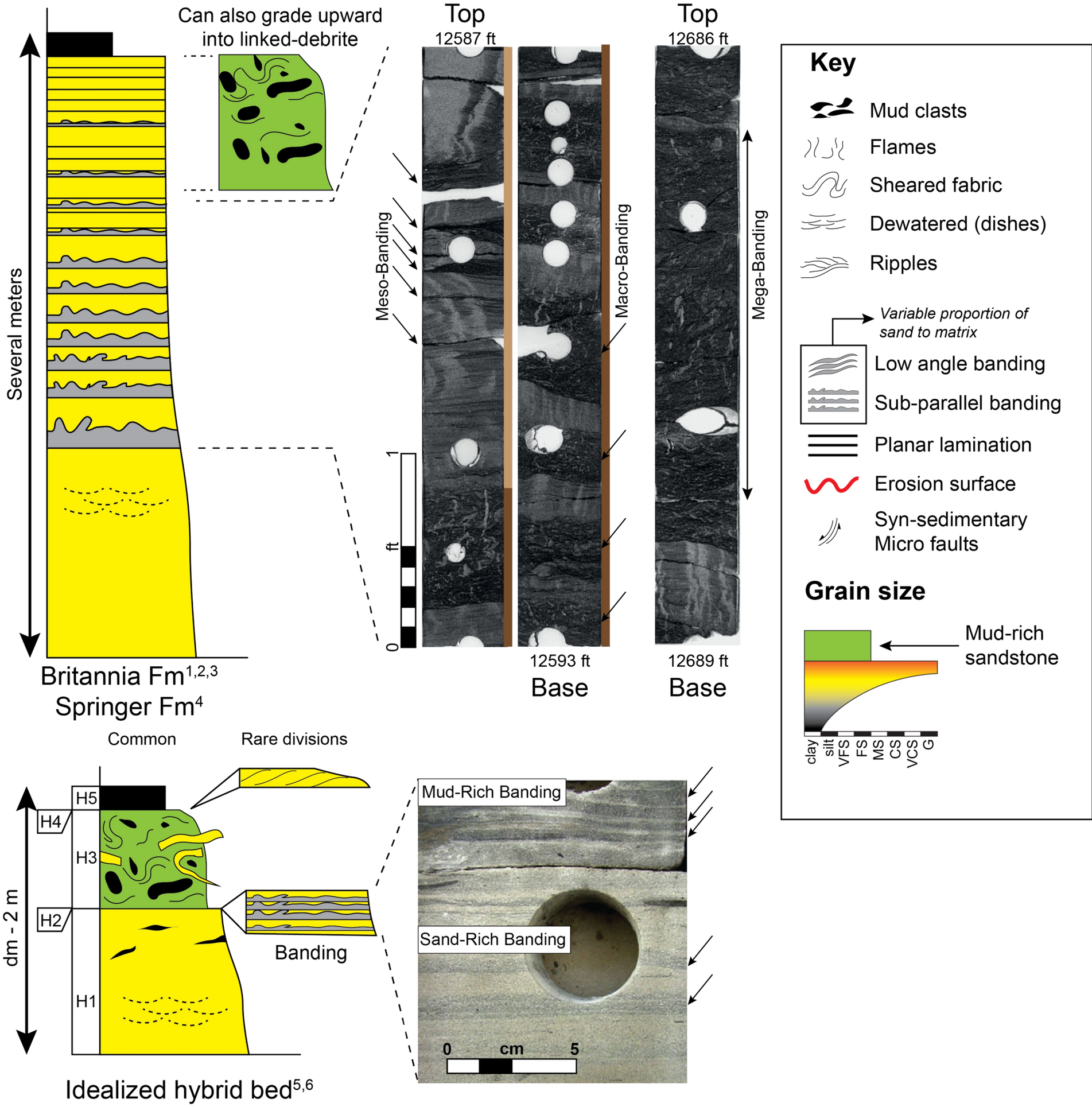
Several meters
Can also grade upward into linked-debrite
Top
12587 ft
Top
12686 ft
Meso-Banding
Macro-Banding
Mega-Banding
1
ft
0
12593 ft
Base
12689 ft
Base
Britannia Fm[1,2,3]
Springer Fm[4]
Key
Mud clasts
Flames
Sheared fabric
Dewatered (dishes)
Ripples
Variable proportion of sand to matrix
Low angle banding
Sub-parallel banding
Planar lamination
Erosion surface
Syn-sedimentary Micro faults
Grain size
Mud-rich sandstone
clay
silt
VFS
FS
MS
CS
VCS
G
Common
Rare divisions
H5
H4
H3
H2
H1
dm - 2 m
Banding
Mud-Rich Banding
Sand-Rich Banding
0
cm
5
Idealized hybrid bed[5,6]

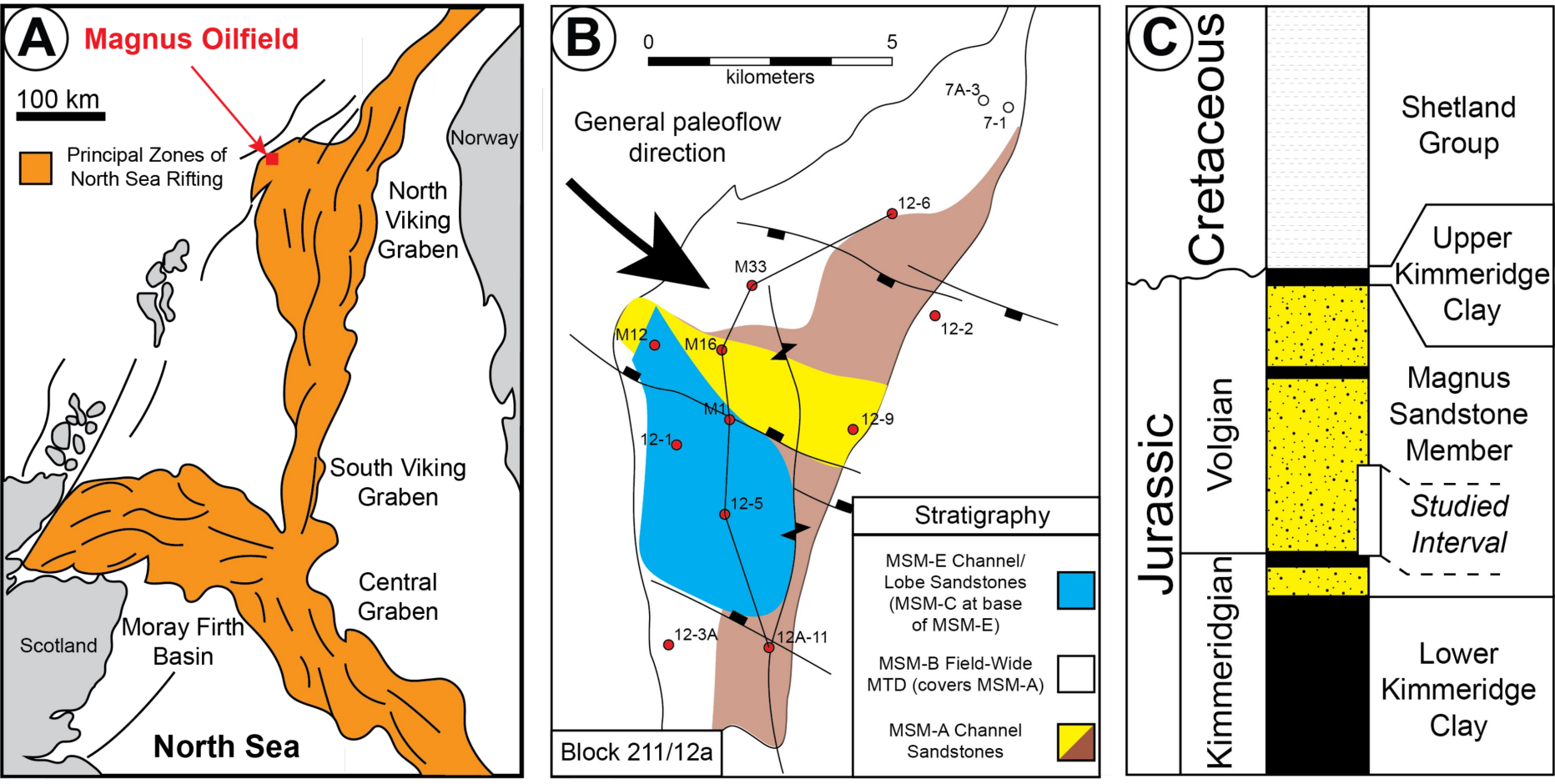
A
Magnus Oilfield
100 km
Principal Zones of North Sea Rifting
Norway
North Viking Graben
South Viking Graben
Central Graben
Moray Firth Basin
Scotland
North Sea
B
0
5
kilometers
General paleoflow direction
7A-3
7-1
12-6
M33
12-2
M12
M16
M1
12-9
12-1
12-5
12-3A
12A-11
Block 211/12a
Stratigraphy
MSM-E Channel/ Lobe Sandstones (MSM-C at base of MSM-E)
MSM-B Field-Wide MTD (covers MSM-A)
MSM-A Channel Sandstones
C
Cretaceous
Jurassic
Volgian
Kimmeridgian
Shetland Group
Upper Kimmeridge Clay
Magnus Sandstone Member
Studied Interval
Lower Kimmeridge Clay

Figure 2

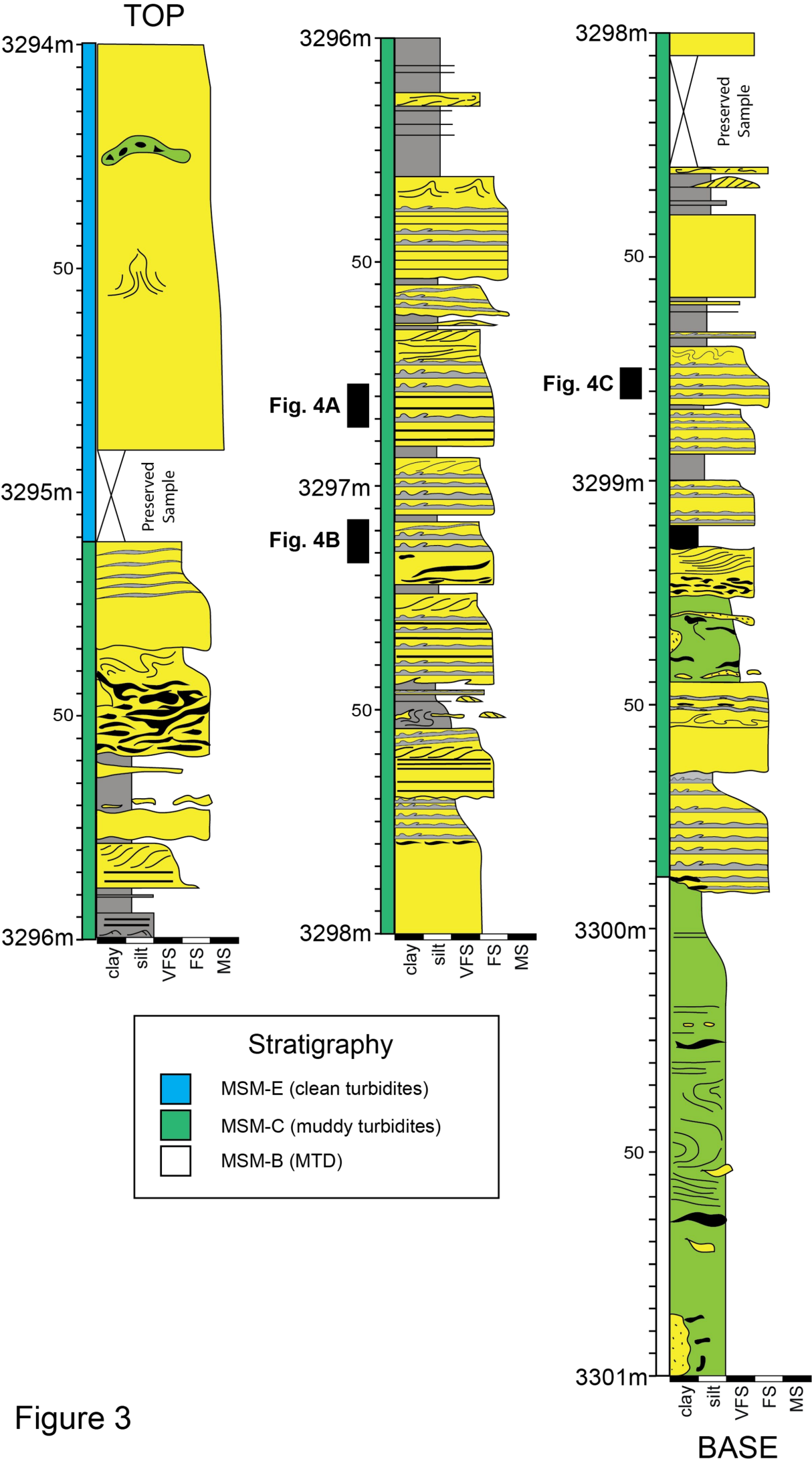
TOP
3294m
50
3295m
Preserved Sample
50
3296m
clay
silt
VFS
FS
MS
3296m
50
Fig. 4A
3297m
Fig. 4B
50
3298m
clay
silt
VFS
FS
MS
3298m
Preserved Sample
50
Fig. 4C
3299m
50
3300m
50
3301m
clay
silt
VFS
FS
MS
BASE
Stratigraphy
MSM-E (clean turbidites)
MSM-C (muddy turbidites)
MSM-B (MTD)

Figure 3

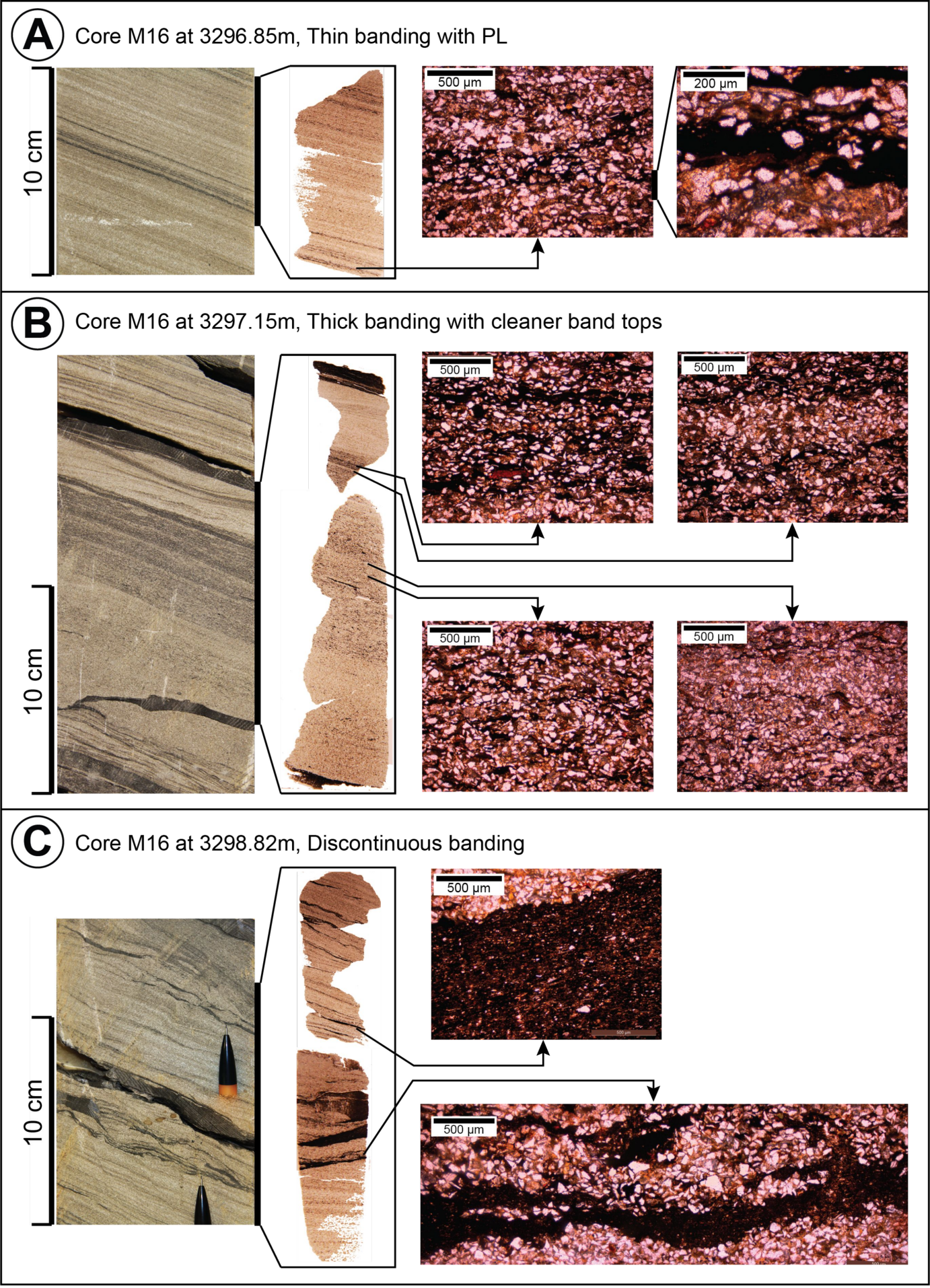
A
Core M16 at 3296.85m, Thin banding with PL
10 cm
500 µm
200 µm
B
Core M16 at 3297.15m, Thick banding with cleaner band tops
10 cm
500 µm
500 µm
500 µm
500 µm
C
Core M16 at 3298.82m, Discontinuous banding
10 cm
500 µm
500 µm

Figure 4

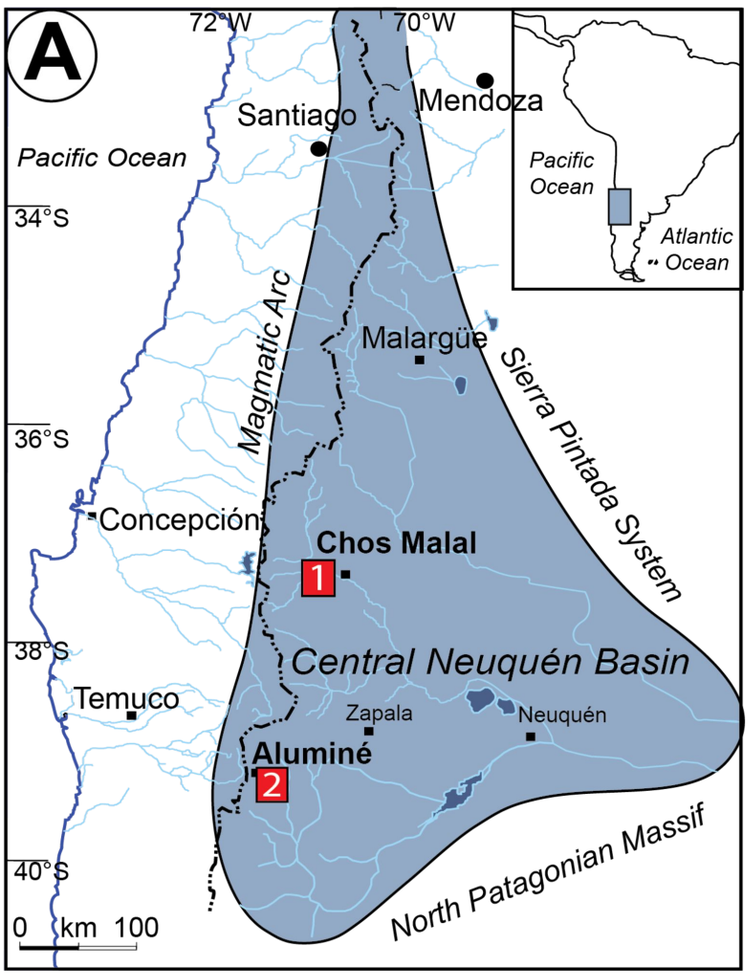
A
72°W
70°W
Santiago
Mendoza
Pacific Ocean
34°S
Pacific Ocean
Atlantic Ocean
Magmatic Arc
Malargüe
Sierra Pintada System
36°S
Concepción
Chos Malal
1
38°S
Central Neuquén Basin
Temuco
Zapala
Neuquén
Aluminé
2
40°S
North Patagonian Massif
0 km 100


1
N
Cordillera del Viento
Chacay Melehue
5 km


2
N
Co. Panqueco
Jardinera
Cuesta
5 km

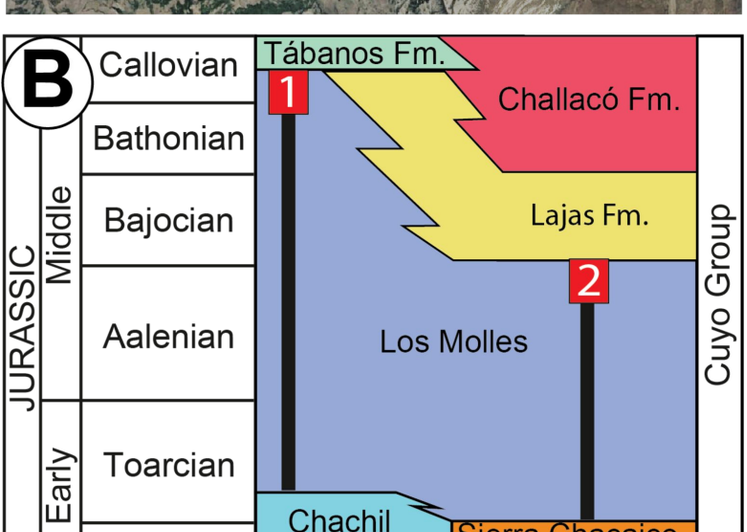
B
JURASSIC
Middle
Early
Callovian
Bathonian
Bajocian
Aalenian
Toarcian
Tábanos Fm.
1
Challacó Fm.
Lajas Fm.
2
Los Molles
Cuyo Group
Chachil
Sierra Chacaico

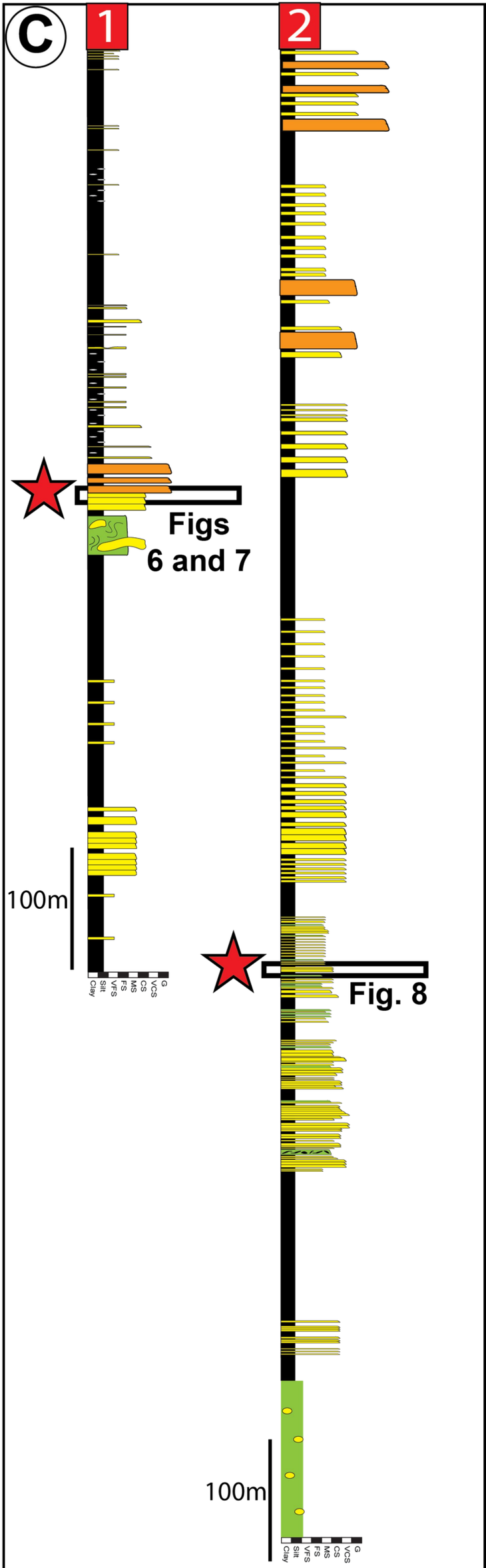
C
1
2
Figs 6 and 7
100m
Clay
Silt
VFS
FS
MS
CS
VCS
G
Fig. 8
100m

Figure 5

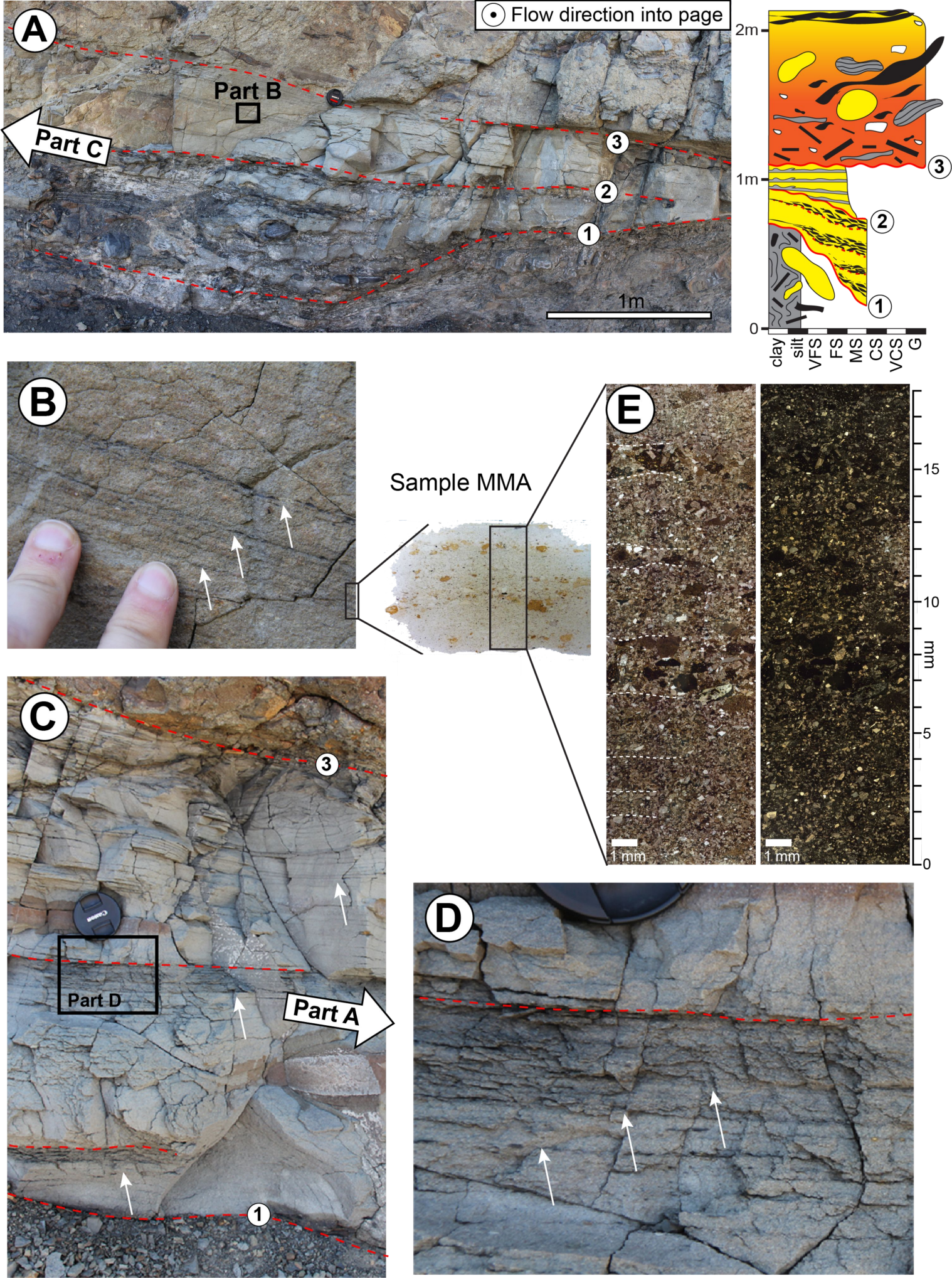
A
Flow direction into page
Part B
Part C
3
2
1
1m
2m
1m
0
clay
silt
VFS
FS
MS
CS
VCS
G
B
Sample MMA
E
15
10
mm
5
0
1 mm
1 mm
C
3
Part D
Part A
1
D

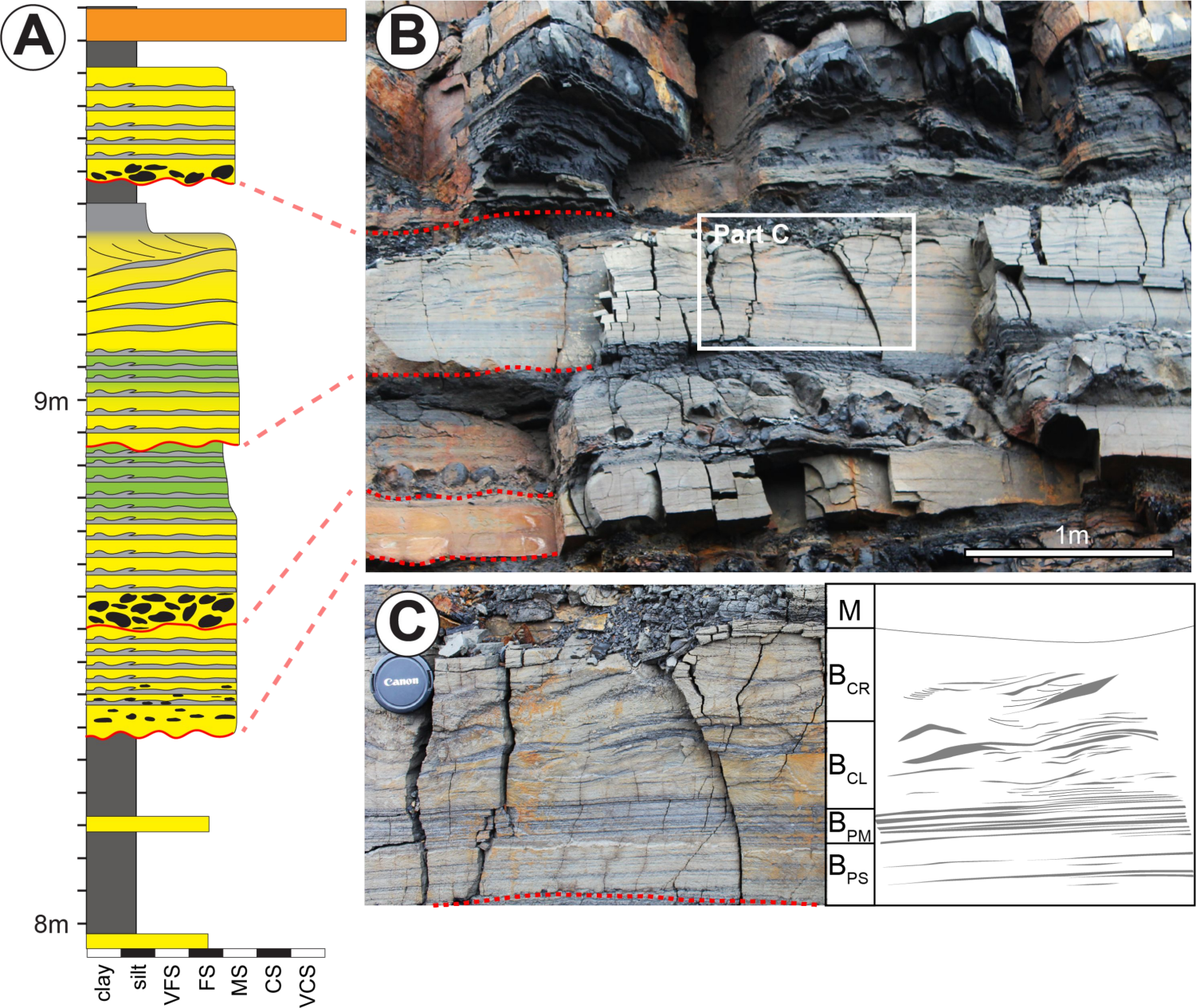
A
9m
8m
clay
silt
VFS
FS
MS
CS
VCS
B
Part C
1m
C
Canon
M
B CR
B CL
B PM
B PS

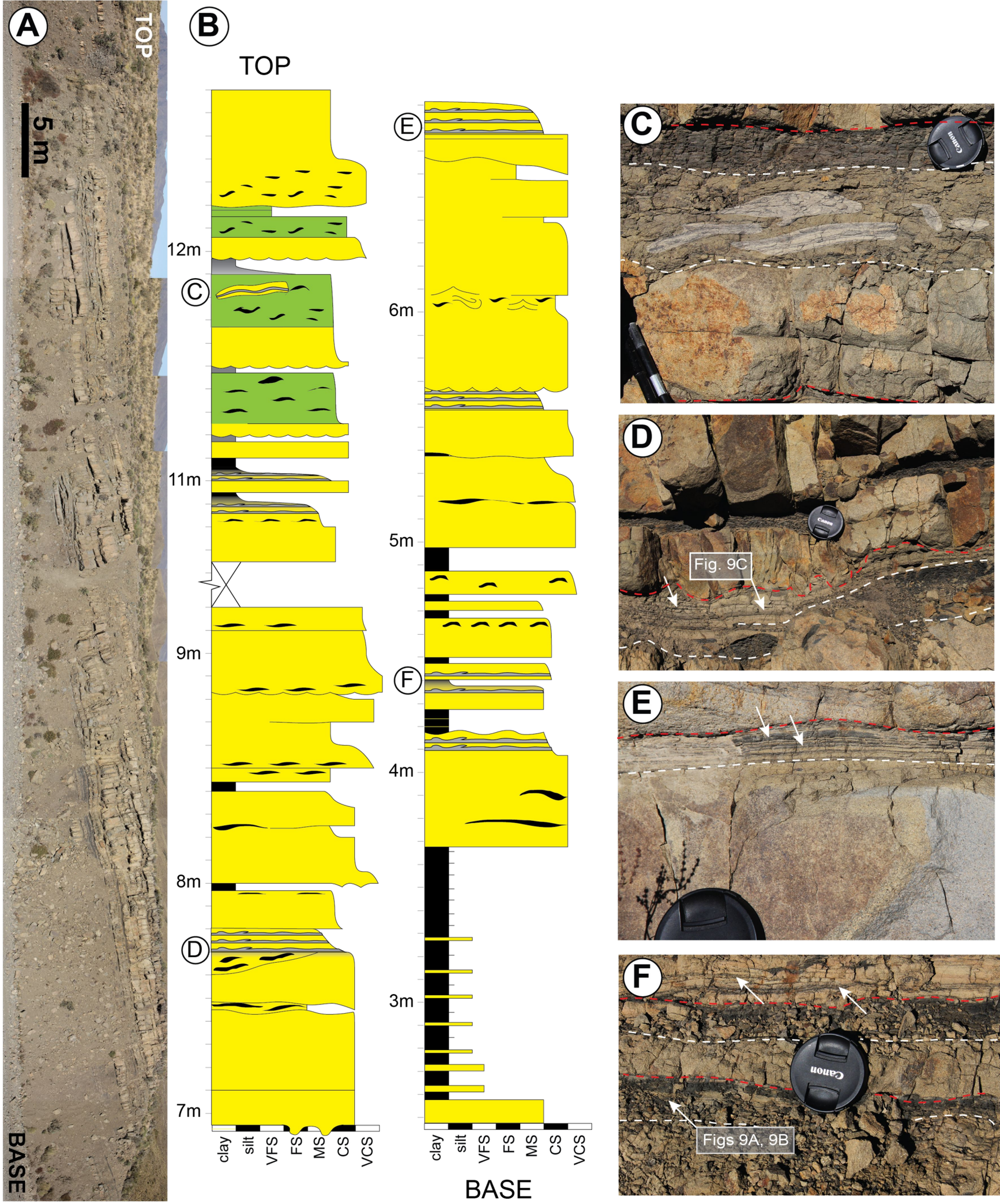
A
TOP
5 m
BASE
B
TOP
12m
C
11m
9m
8m
D
7m
clay
silt
VFS
FS
MS
CS
VCS
E
6m
5m
F
4m
3m
clay
silt
VFS
FS
MS
CS
VCS
BASE
C
D
Fig. 9C
E
F
Figs 9A, 9B

Figure 8

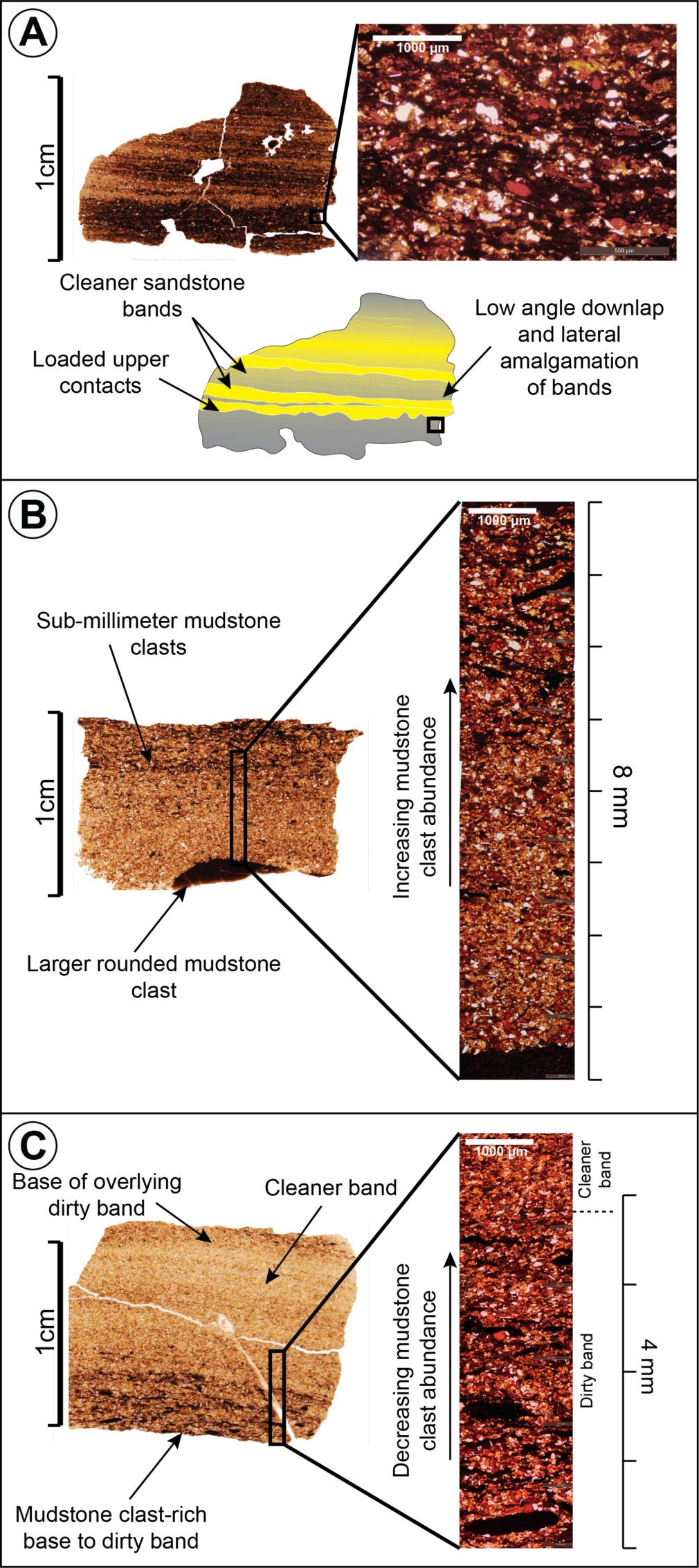
A
1cm
1000 µm
Cleaner sandstone bands
Loaded upper contacts
Low angle downlap and lateral amalgamation of bands
B
Sub-millimeter mudstone clasts
1cm
Larger rounded mudstone clast
1000 µm
Increasing mudstone clast abundance
8 mm
C
Base of overlying dirty band
Cleaner band
1cm
Mudstone clast-rich base to dirty band
1000 µm
Decreasing mudstone clast abundance
Cleaner band
Dirty band
4 mm

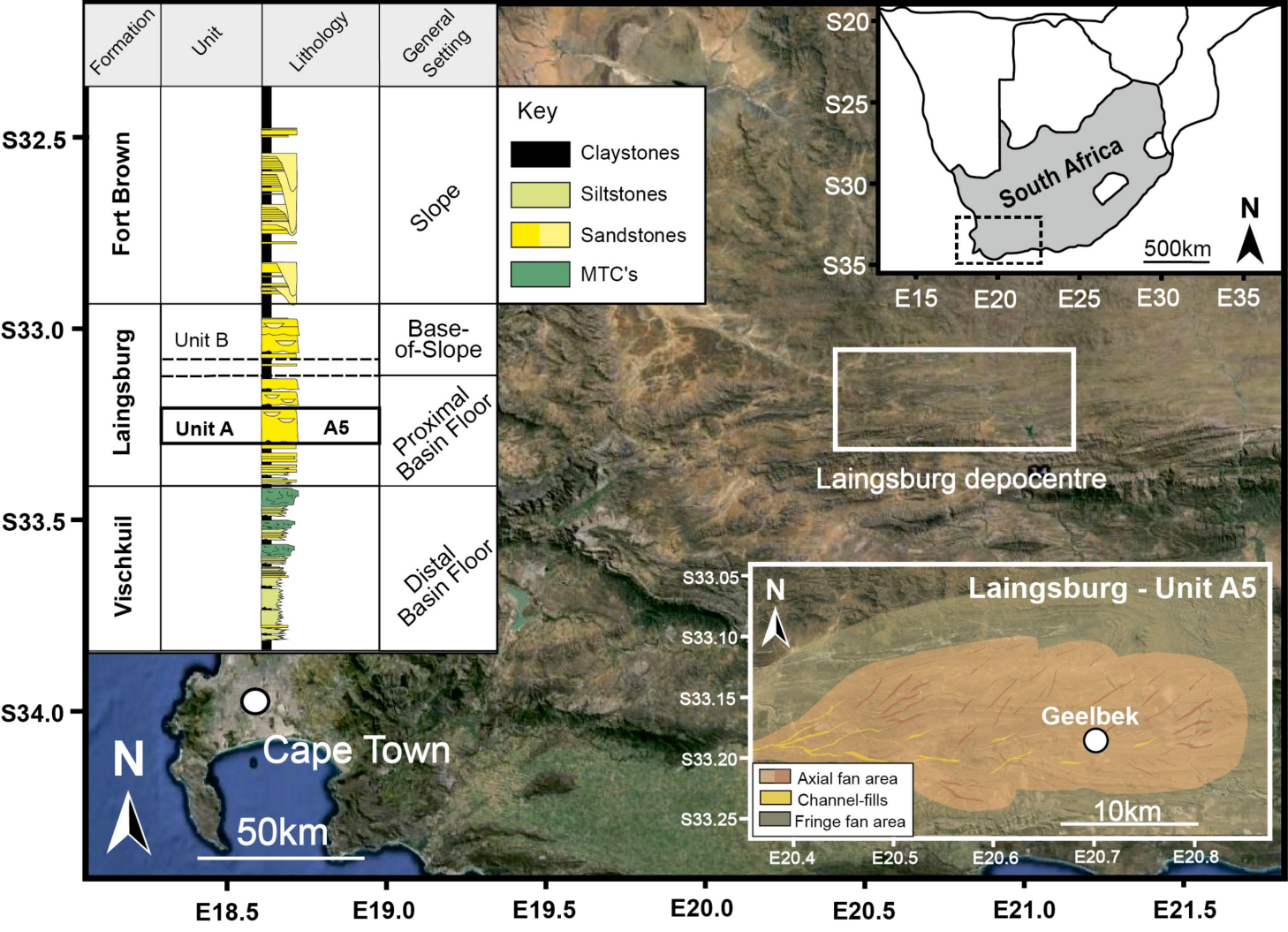
Formation
Unit
Lithology
General Setting
Fort Brown
Laingsburg
Vischkuil
Unit B
Unit A
A5
Slope
Base-of-Slope
Proximal Basin Floor
Distal Basin Floor
Key
Claystones
Siltstones
Sandstones
MTC's
S32.5
S33.0
S33.5
S34.0
S20
S25
S30
S35
E15
E20
E25
E30
E35
South Africa
N
500km
Laingsburg depocentre
S33.05
S33.10
S33.15
S33.20
S33.25
Laingsburg - Unit A5
Geelbek
Axial fan area
Channel-fills
Fringe fan area
10km
E20.4
E20.5
E20.6
E20.7
E20.8
Cape Town
50km
E18.5
E19.0
E19.5
E20.0
E20.5
E21.0
E21.5

Figure10

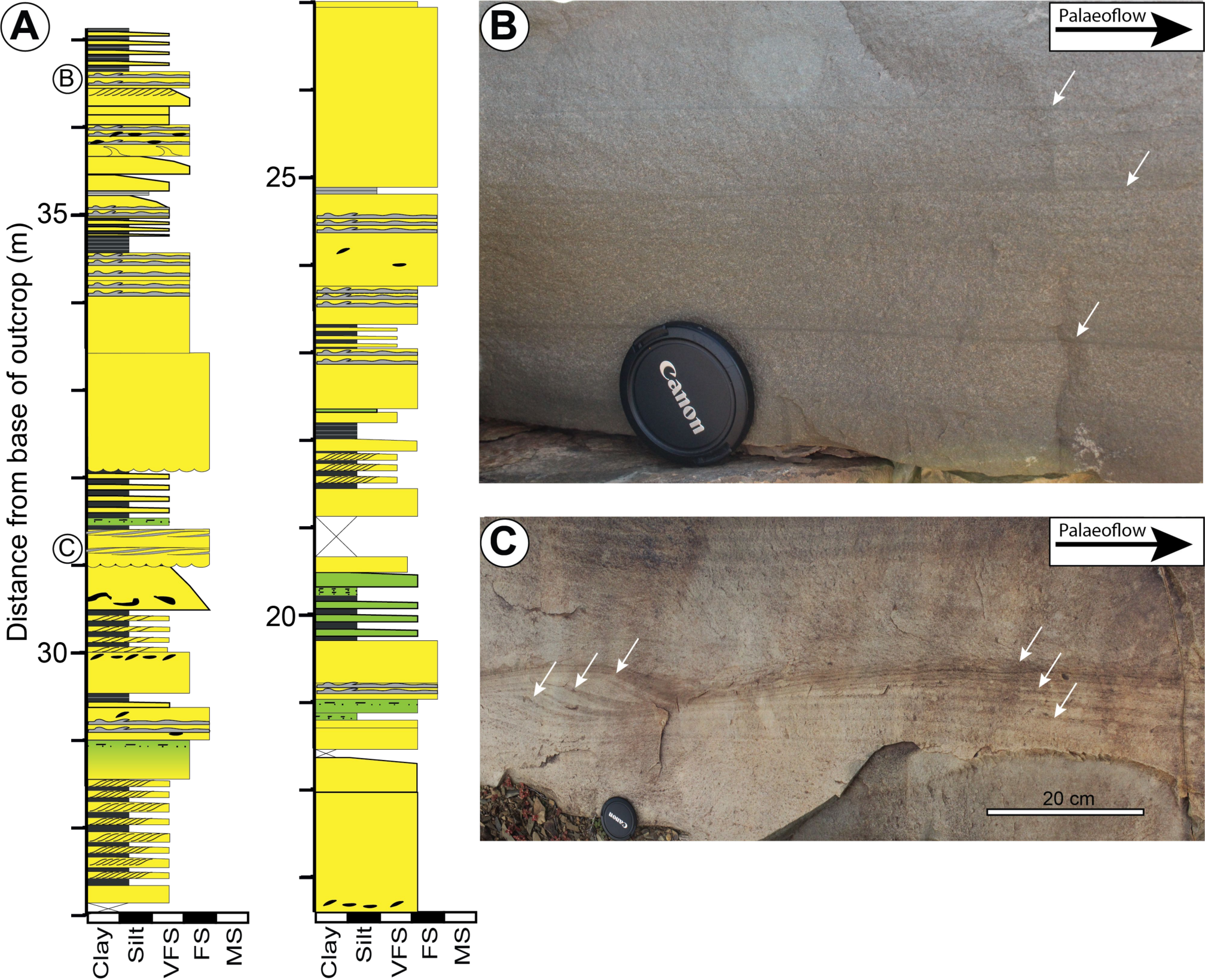
A
B
C
35
30
25
20
Distance from base of outcrop (m)
Clay
Silt
VFS
FS
MS
Clay
Silt
VFS
FS
MS
B
Palaeoflow
Canon
C
Palaeoflow
20 cm

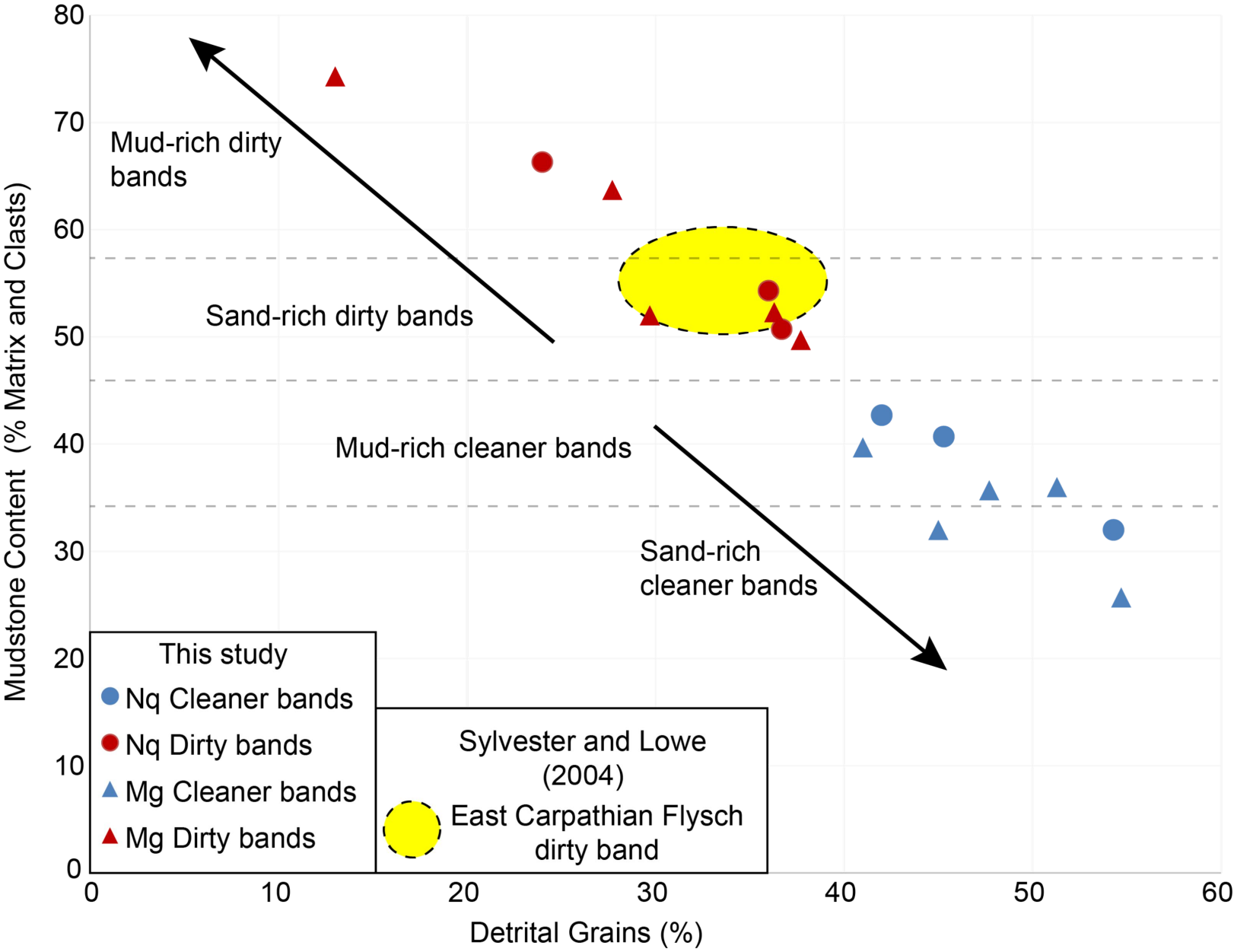
Mudstone Content (% Matrix and Clasts)
Detrital Grains (%)
0
10
20
30
40
50
60
70
80
Mud-rich dirty bands
Sand-rich dirty bands
Mud-rich cleaner bands
Sand-rich cleaner bands
This study
Nq Cleaner bands
Nq Dirty bands
Mg Cleaner bands
Mg Dirty bands
Sylvester and Lowe (2004)
East Carpathian Flysch dirty band

Field Deposits

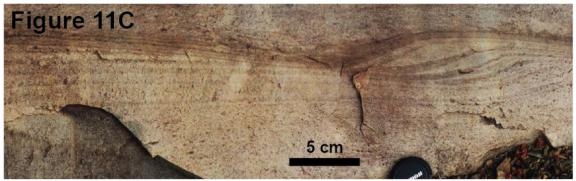

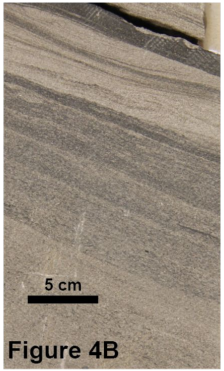

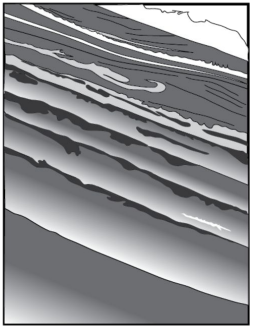

Experimental Deposits

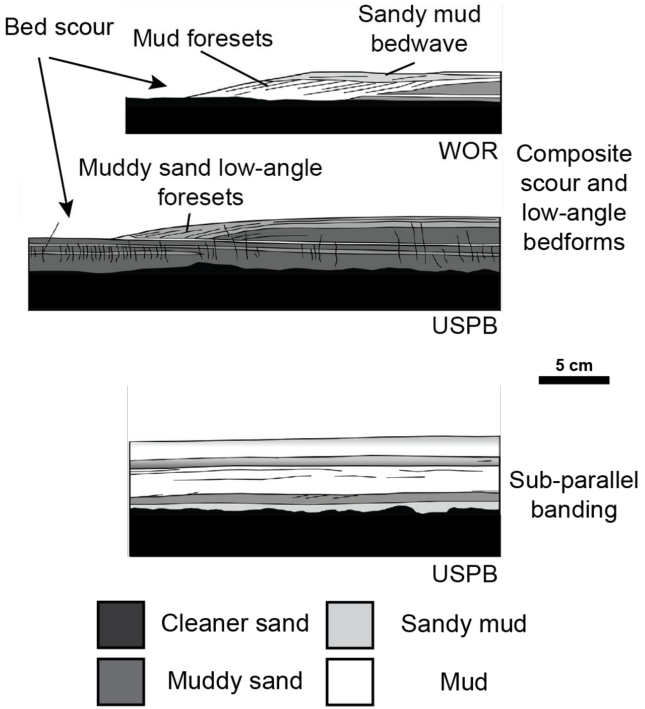

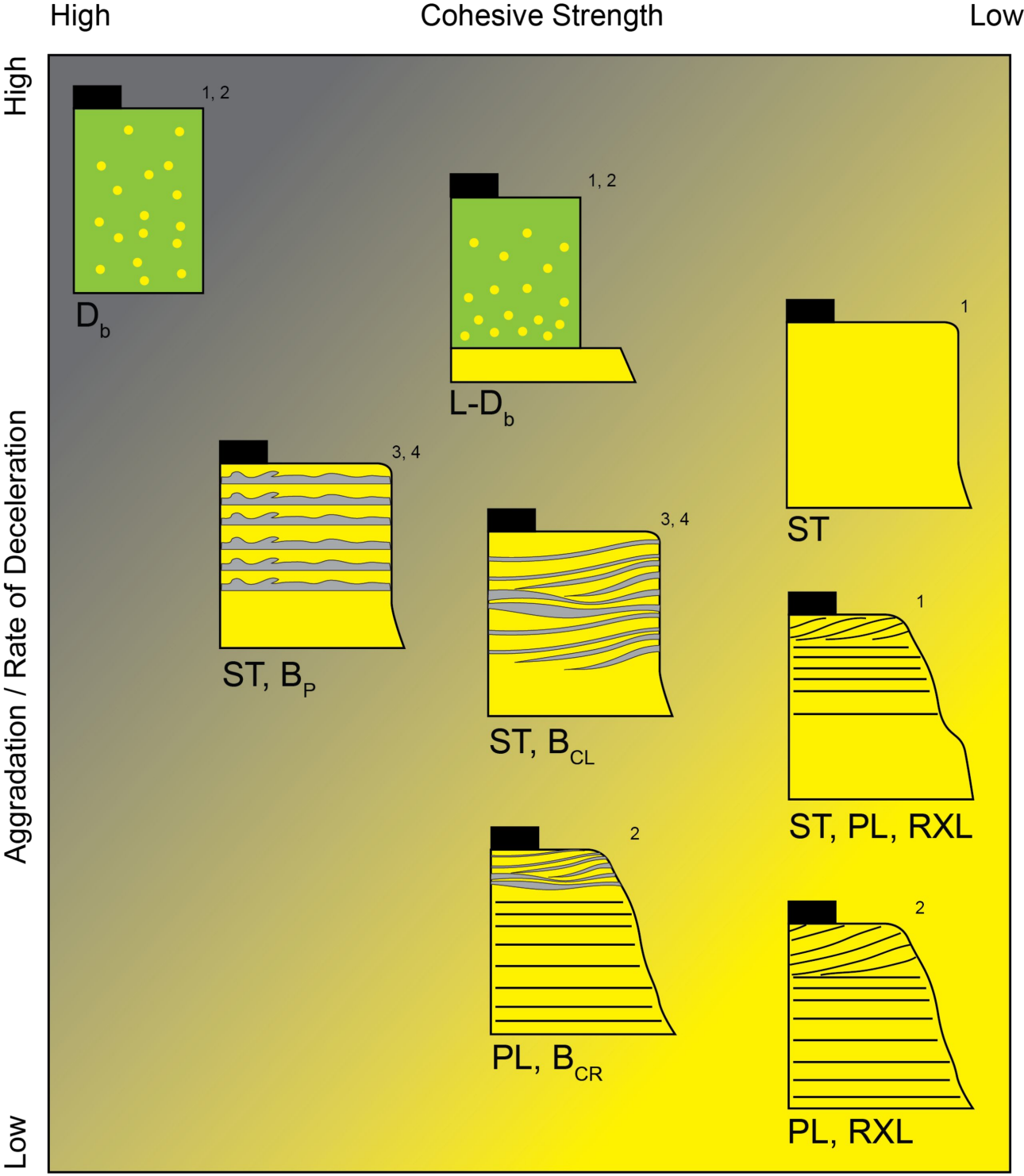
High
Cohesive Strength
Low
High
Aggradation / Rate of Deceleration
Low
1, 2
D b
1, 2
L-D b
1
ST
3, 4
ST, B P
3, 4
ST, B CL
1
ST, PL, RXL
2
PL, B CR
2
PL, RXL

Figure 14

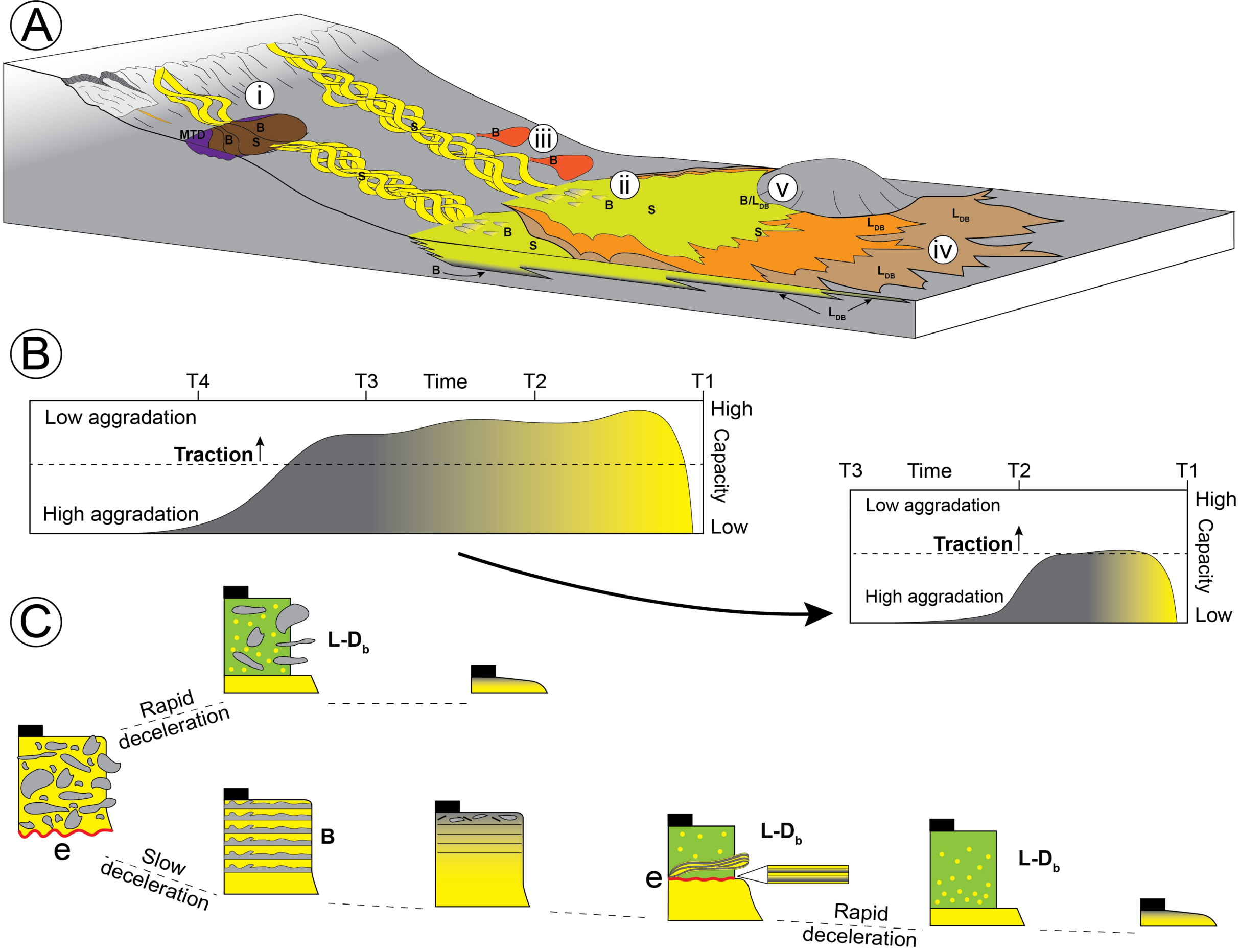
A
i
ii
iii
iv
v
MTD
B
S
B/L_DB
L_DB
B
T4
T3
Time
T2
T1
Low aggradation
Traction
High aggradation
High
Capacity
Low
T3
Time
T2
T1
Low aggradation
Traction
High aggradation
High
Capacity
Low
C
L-D_b
Rapid deceleration
e
Slow deceleration
B
L-D_b
e
Rapid deceleration
L-D_b
Facies
S - Clean sandstone
B - Banded sandstone
L-D_B - Linked-debrite
MTD - Mass transport deposit
Environment
Channels
Channel-splay
Intraslope lobe
Proximal lobe
Medial lobe
Distal lobe
Hemipelagic
Symbols
Sandstone/mudstone
Muddy sandstone (debrite)
Mudstone clasts
Banded sandstone clasts
Banded sandstone
Parallel lamination
Erosion

Figure 15